https://ntrs.nasa.gov/search.jsp?R=19780003109 2020-03-22T07:12:45+00:00Z

NASA TECHNICAL MEMORANDUM

NASA TM X-3561

NASA TM X-3561

CASE FILE COPY

EXPERIMENTAL AND ANALYTICAL DETERMINATION OF CHARACTERISTICS AFFECTING LIGHT AIRCRAFT LANDING-GEAR DYNAMICS

Edwin L. Fasanella, John R. McGehee, and M. Susan Pappas

Langley Research Center
Hampton, Va. 23665

NATIONAL AERONAUTICS AND SPACE ADMINISTRATION • WASHINGTON, D. C. • NOVEMBER 1977

1. Report No.	2. Government Accession No.	3. Recipient's Catalog No.
NASA TM X-3561		

4. Title and Subtitle	5. Report Date
EXPERIMENTAL AND ANALYTICAL DETERMINATION OF CHARACTERISTICS AFFECTING LIGHT AIRCRAFT LANDING-GEAR DYNAMICS	November 1977
	6. Performing Organization Code
7. Author(s)	8. Performing Organization Report No.
Edwin L. Fasanella, John R. McGehee, and M. Susan Pappas	L-11472
	10. Work Unit No.
9. Performing Organization Name and Address	743-01-12-03
NASA Langley Research Center Hampton, VA 23665	11. Contract or Grant No.
	13. Type of Report and Period Covered
12. Sponsoring Agency Name and Address	Technical Memorandum
National Aeronautics and Space Administration Washington, DC 20546	14. Sponsoring Agency Code

15. Supplementary Notes

Edwin L. Fasanella: Vought Corporation, Hampton Technical Center, Hampton, Virginia.
John R. McGehee and M. Susan Pappas: Langley Research Center.

16. Abstract

An experimental and analytical investigation was conducted to determine which characteristics of a light aircraft landing gear influence gear dynamic behavior significantly. The investigation focused particularly on possible modification for load control. Pseudostatic tests were conducted to determine the gear fore-and-aft spring constant, axial friction as a function of drag load, brake pressure-torque characteristics, and tire force-deflection characteristics. To study dynamic tire response, vertical drops were conducted at impact velocities of 1.2, 1.5, and 1.8 m/s (4, 5, and 6 ft/s) onto a level surface; to determine axial-friction effects, a second series of vertical drops were made at 1.5 m/s (5 ft/s) onto surfaces inclined 5^{o} and 10^{o} to the horizontal. An average dynamic axial-friction coefficient of 0.15 was obtained by comparing analytical data with inclined surface drop test data. Dynamic strut bending and associated axial friction were found to be severe for the drop tests on the 10^{o} surface.

17. Key Words (Suggested by Author(s))	18. Distribution Statement
Active controls Aircraft landing gear Landing loads	Unclassified – Unlimited Subject Category 05

19. Security Classif. (of this report)	20. Security Classif. (of this page)	21. No. of Pages	22. Price*
Unclassified	Unclassified	44	$4.00

*For sale by the National Technical Information Service, Springfield, Virginia 22161

EXPERIMENTAL AND ANALYTICAL DETERMINATION OF CHARACTERISTICS AFFECTING LIGHT AIRCRAFT LANDING-GEAR DYNAMICS

Edwin L. Fasanella,* John R. McGehee,
and M. Susan Pappas
Langley Research Center

SUMMARY

An experimental and analytical investigation was conducted to determine those characteristics of a light aircraft landing gear, that might influence the gear's dynamic behavior significantly, especially when such a gear is modified to provide load control. The basic investigation consisted of three major phases. In the first phase, pseudostatic tests were conducted to determine the gear's force-and-aft spring constant, gear axial friction as a function of drag load, brake pressure-torque characteristics, and tire force-deflection characteristics. In the second and third phases, the gear was instrumented, and two separate series of dynamic vertical drop tests were made using honeycomb to simulate lift characteristics. The first series of vertical drops was conducted at impact velocities of 1.2, 1.5, and 1.8 m/s (4, 5, and 6 ft/s) onto a level surface while the second series, designed to emphasize axial-friction effects, was carried out at 1.5 m/s (5 ft/s) onto surfaces inclined at 5° and 10° to the horizontal.

The experimental data from level surface drop tests (with honeycomb lift simulation) were in excellent agreement with analytical data for all measured parameters: shock strut stroke, tire deflection, pneumatic pressure, hydraulic pressure, lower mass acceleration, and upper mass acceleration. The honeycomb lift simulation was found to be accurate and reliable for the initial impact. The semiempirical tire equation if hysteresis effects were neglected was accurate for both pseudostatic and dynamic impact conditions.

The gear axial-friction coefficient for the pseudostatic tests was approximately 0.27 and independent of shock strut extension for small drag loads. The dynamic axial-friction coefficient obtained by analytical modeling of the inclined surface drop tests was considerably lower; a value of 0.15 gave the best overall analytical fit to the experimental data.

---

*Vought Corporation, Hampton Technical Center, Hampton, Virginia.

Strut bending and associated axial friction for the 10^{o} inclined surface drop tests were more severe than had been anticipated. Experimentally, the vertical hub acceleration experienced a large oscillation of approximately 23 Hz after the main impact peak. The pseudostatic spring constant showed that this oscillation frequency corresponded approximately to the natural fore-and-aft bending frequency of the gear. Consequently, under extreme conditions the fore-and-aft bending of the gear can affect both gear axial friction and gear dynamics considerably.

INTRODUCTION

In large aircraft, dynamic loads and vibrations resulting from landing impact and from runway and taxiway unevenness are recognized as significant factors in causing fatigue damage, dynamic stress on the airframe structure, crew and passenger discomfort, and reduction of the pilot's ability to control the aircraft. These ground-induced dynamic loads and vibration problems have been encountered with some conventional transport aircraft (refs. 1 and 2) and are magnified for supersonic-cruise aircraft because of increased structural flexibility of the slender-body, thin-wing designs and the higher take-off and landing speeds. One potential method for improving ground operational characteristics of supersonic-cruise aircraft is the application of active control technology to landing gears to limit the loads applied to the airframe.

The study described in reference 3 concerned the feasibility of applying active controls to aircraft landing gears by means of a mathematical model of an active control gear. During the analytical study of a series-hydraulic active control concept carried out in that investigation, the strut axial-friction force was found to have a significant influence on control performance. Since the strut axial-friction force is influenced by tire force and strut bending produced by drag and side loads from braking and cornering, a definition of binding friction characteristics for a specific gear is required for design of a compatible active control system. This paper offers a definition of these characteristics for a landing gear from a 2720-kg (6000-lbm) class aircraft. (Values are given in both SI and U.S. Customary Units. Measurements were made in U.S. Customary Units.)

The investigation consisted of three major phases. In the first phase, experimental pseudostatic (slowly varying) tests were made to determine the shock strut fore-and-aft spring constant as a function of strut extension, axial friction as a function of drag load and strut extension, tire force-deflection characteristics, and brake pressure-torque characteristics. In the second and third phases, two series of dynamic vertical drop tests were performed, and the experimental values obtained were compared with analytical predictions using computer program active control landing gear analysis (ACOLAG; see ref. 3).

In the first series of vertical drop tests (second phase) conducted at 1.2, 1.5, and 1.8 m/s (4, 5, and 6 ft/s) onto a level impact surface, the axial gear friction force was assumed to be 0 (except for a small fit friction term) due to the absence of a force normal to the gear. With the effects of friction removed, attention was directed to the tire force-deflection characteristics to ascertain whether the analytical model (using a semi-empirical equation from ref. 4) could predict the experimental dynamic tire response.

The second series of vertical drop tests (third phase) was made at 1.5 m/s (5 ft/s) onto surfaces inclined at 5° and 10° to the horizontal. These tests were designed to emphasize the effects of axial strut friction and strut fore-and-aft bending for dynamic impact conditions. The magnitude of the dynamic axial-friction coefficient was determined by comparing analytical predictions with the drop test data. The effects of fore-and-aft strut bending on the axial friction were also investigated experimentally, although the effect was not analytically modeled.

LANDING GEAR

A cross section and details of the gear employed in this experiment are shown in figure 1. The gear is a conventional oleo-pneumatic main landing gear designed for a 2720-kg (6000-lbm) class, fixed wing aircraft. The wheel, equipped with disc brakes, is fitted with an 8-ply, 6.50-10, type III aircraft tire rated at a maximum load of 16.68 kN (3750 lbf) and maximum inflation pressure of 550 kPa (80 psig). Appendix A presents the pertinent gear geometric characteristics.

APPARATUS

Apparatus, test setup, and procedure used for the pseudostatic tests are presented in appendix B. A special fixture was designed to attach directly to the gear for mounting the gear to the vertical backstop for the pseudostatic tests and to the drop carriage for the dynamic vertical drop tests. The apparatus used for the dynamic vertical drop tests is described in the section immediately following.

Drop Rig

For the vertical drop tests, the gear and its mounting fixture were bolted to the drop carriage as shown in figure 2. The 1220-kg (2700-lbm) movable section (drop carriage), guided vertically by track and rollers, was raised by an overhead crane to the height necessary for the desired gear impact velocity. Ballast was added to increase the mass of the drop carriage to 1490 kg (3280 lbm), approximately one-half the mass of the aircraft, and was positioned to bring the center of gravity of the mass directly over the line of action of the landing gear. To minimize moments that tended to bind the rollers on the

tracks, the gear was mounted as near the backstop as feasible. A bomb release mechanism was electrically activated to initiate each drop test.

Lift Simulation

Previous investigators have employed various means to simulate lift during a vertical drop test. Among these methods were reduced drop mass (ref. 5) and hydraulic or pneumatic constant force devices. For the present investigation, aluminum honeycomb (Hexcel 1/4-5052-0.001P) was chosen for its simplicity, accuracy, and repeatability as a constant force generator with desirable (small) rebound characteristics. Honeycomb blocks 25.4 cm (10.0 in.) high, 26.2 cm (10.3 in.) long, and 10.2 cm (4.0 in.) wide were precrushed in a materials testing machine which plotted the steady-state force level. The blocks chosen for the impact tests crushed with a constant force level of about 16.00 kN (3600 lbf). The average force per cell was computed, and blocks which crushed above the desired force level could be brought into the correct range by removing the required number of cells.

The honeycomb force does not decay steadily to 0 as aerodynamic lift would in an actual landing. The honeycomb force is either "off" or "on." Thus honeycomb used as a lift simulator is representative of aerodynamic lift only for the time interval between honeycomb impact and the time the upper mass velocity reverses (rebounds from honeycomb). At this time the honeycomb force rapidly falls to 0, leaving the gravitational force again unbalanced. The consequent loading and unloading of the honeycomb causes an oscillation in the upper mass acceleration.

Inclined Surfaces

Two inclined surfaces were constructed with 5° and 10° angles of inclination. The impact surface of 0.95-cm (3/8-in.) thick aluminum was bolted to wedge-shaped hardwood strips to give the desired inclination angle. A drawing of a vertical drop test setup with an inclined impact surface is shown in figure 3.

DYNAMIC VERTICAL DROP TEST PROCEDURE

The pre-drop preparation of the gear was the same for all dynamic vertical drop tests. The fully extended gear with valve core removed was filled with hydraulic fluid conforming to MIL-H-5606 specifications. The gear was stroked, extended, filled, and stroked again to force out entrapped air. The gear cylinder valve core was replaced and nitrogen gas was added until the gear extended 8.26 cm $\left(3\frac{1}{4}\text{ in.}\right)$ while supporting the 1490-kg (3280-lbm) drop mass. With this procedure the resulting pneumatic gauge pressure for the fully extended gear was 1917 ± 69 kPa (278 ± 10 psig). The tire was inflated to 414 kPa (60 psig) for all tests.

Before each group of drops the drop height above the honeycomb was adjusted to give the desired impact velocity. Only a 17.0-cm (6.7-in.) drop is required for the gear to accelerate, under gravity, to an impact velocity of 1.8 m/s (6 ft/s). Honeycomb crush from 2.54 cm (1.0 in.) to 5.08 cm (2.0 in.) was allowed before tire contact. Since the honeycomb force was chosen to approximately balance the total weight, the gear velocity remained approximately constant for the interval between honeycomb impact and tire contact. This period of time also allowed the accelerometer signal oscillations created by honeycomb impact to dampen appreciably before tire impact.

The gear and tire pressures were checked before each drop test as was the position of the hub displacement potentiometer at tire contact. To establish the impact velocity, a gauge was used to measure the drop height above the honeycomb. When necessary, shims were placed under the honeycomb column to correct the drop height.

The vertical drop tests on the level surface consisted of three drops at each impact velocity: 1.2 m/s (4 ft/s), 1.5 m/s (5 ft/s), and 1.8 m/s (6 ft/s). The greatest impact velocity chosen was 1.8 m/s (6 ft/s) because of the small probability of occurrence of higher velocities during actual aircraft landings (ref. 6).

For the vertical drop tests on the inclined surfaces, three drops at an impact velocity of 1.5 m/s (5 ft/s) were made on each of the 5° and 10° surfaces. Before and after these tests, drops were made on a flat level surface to assure repeatability with the first series of tests.

VERTICAL DROP INSTRUMENTATION

Instrumentation provided time histories of upper mass acceleration, hub acceleration, hydraulic pressure, pneumatic pressure, shock strut stroke, and tire deflection. To alleviate dynamic response errors, electronic filtering flat to 100 Hz was used for the signals from the accelerometer and the pressure transducers.

Two dc servo accelerometers were used to measure hub and upper mass accelerations in the vertical direction. The upper mass accelerometer had a ±5g range with a 650-Hz natural frequency. (1g = 9.80 m/s^2 (32 ft/s^2).) The hub accelerometer range was ±25g with a natural frequency of 770 Hz. Both accelerometers had 0.05-percent full-scale linearity, near 0 hysteresis (0.0005g), and 0 cross coupling coefficient (pendulosity error). A 2g calibration was made by rotating the accelerometers 180° (from up to down) in the Earth's gravity field at sea level elevation. A downward direction was chosen for positive acceleration.

The pneumatic pressure transducer was mounted in the upper part of the cylinder. The hydraulic pressure transducer was mounted in the piston plug as shown in figure 4. Removing the air valve core, pressurizing the gear with dry nitrogen, and monitoring the pressure with a dead weight pressure calibrator allowed both pressure transducers to be

calibrated simultaneously from 0 to 42 kPa (0 to 600 psig) while in the gear. The two strain-gauge pressure transducers ranged from 0 to 13 790 kPa (0 to 2000 psig). Two variable resistance slide-wire potentiometers capable of 30.5-cm (12.0-in.) total travel were used to measure strut stroke and vertical tire deflection. (See fig. 2.)

Outputs from all transducers were recorded on the oscillograph shown in figure 5. An electronic timer generated timing lines on the oscillograph record at 0.01-s intervals.

High-speed motion pictures (400 frames/s) of each drop enabled a motion analyzer to be used for independent determination of impact velocity and strut stroke. A 60-Hz signal was recorded on the border of the film as a time code for establishing frame rate.

ANALYTICAL SIMULATION

The physical characteristics of the gear (appendix A), the empirical tire properties, and the proper initial conditions were input into computer program active control landing gear analysis (ACOLAG) (see ref. 3). The passive, vertical drop option was used so that analytical predictions could be compared with the experimental vertical drop tests. In the vertical drop option, ACOLAG solves a coupled two-body problem. The system is composed of the upper mass which includes the drop carriage and the gear cylinder and the lower (hub) mass composed of the wheel, tire, and gear piston. The forces acting on the system are lift (honeycomb force), gravity, friction in the drop carriage rollers, tire force, and the shock strut force. The shock strut force consists of hydraulic, pneumatic, and axial-friction terms and acts on both the upper mass and the hub in equal magnitudes but in opposite directions.

The shock strut axial friction F_f is computed in ACOLAG with a constant friction coefficient assumed. In this particular analysis the upper and lower bearing friction coefficients were input as the same value, and the general formula used in ACOLAG reduces to (see appendix B)

$$F_f = C_f D\left(\frac{2\ell_D}{\ell_1} + 1\right)$$

where

F_f shock strut axial-friction force, N (lbf)

C_f bearing friction coefficient

D force normal to gear at hub (drag load), N (lbf)

ℓ_D distance from lower bearing to hub, cm (in.)

ℓ_1 distance between upper and lower bearings, cm (in.)

The axial-friction term always opposes shock strut motion and changes sign (direction) when the shock strut velocity reverses. Discontinuities are avoided when the hyperbolic tangent operating as a multiplying factor causes the friction force to pass through 0 when the velocity changes sign. The expression used is $\left|\tanh\left(aU_{SS}\right)\right|$ where a is a constant and U_{SS} is the shock strut velocity.

The aerodynamic subroutine in ACOLAG was expanded to model the new simulated lift (honeycomb crush force) used in the drop tests. The variation of honeycomb force with displacement (crush) was modeled as a trapezoid with an onset and offset rate that could be varied to match experimental data. Programming logic to model loading and unloading in both the elastic and plastic range of the honeycomb crush force was included.

RESULTS AND DISCUSSION

Pseudostatic tests were conducted as the first phase of this investigation. The axial friction data obtained from these tests were suspect and consequently dynamic tests were made to determine the axial friction. Data obtained in the pseudostatic and dynamic tests are presented in figures 6 through 13.

Pseudostatic Tests

The first phase of this study consisted of pseudostatic tests to determine the gear fore-and-aft spring constant, brake torque as a function of brake pressure, tire force deflection, and gear axial friction as a function of drag load. Details of the test setup, procedure, and instrumentation are given in appendix B.

The fore-and-aft spring constant was evaluated for 10-, 50-, and 90-percent extensions of the shock strut. The spring constant was found to vary in an approximately linear fashion from 342 kN/m (23 400 lbf/ft) for 90-percent extension of the shock strut to 644 kN/m (44 100 lbf/ft) for a 10-percent extension (fig. 8). Since this test was static, the drag load was limited to 6.23 kN (1400 lbf) to avoid possible damage to the gear.

The relation of brake torque to brake pressure (fig. 9) was linear with a slope of 0.00023 N-m/Pa (1.18 lbf-ft/psig) over the range investigated. Maximum brake torque developed was 2640 N-m (1950 lbf-ft) corresponding to a brake pressure of 11 720 kPa (1700 psig). The values of brake torque from this investigation are for static conditions and are probably reduced under dynamic braking conditions.

Nonrolling tire force as a function of deflection was determined experimentally for forces up to 13.34 kN (3000 lbf). The experimental values fit the semiempirical formula (ref. 4) closely for this type of tire (8 ply, 650-10, type III aircraft tire). (See fig. 10.) Although the unloading was slow (pseudostatic) a small amount of hysteresis was noted for the unloading cycle.

The variation of gear axial-friction force with drag load was also determined for 10-, 50-, and 90-percent extensions of the shock strut (fig. 11). The points were fit to the analytical expression given in appendix B for each of the three extensions in order to evaluate the axial-friction coefficient. The gear axial-friction coefficient was found to be approximately 0.27. The value was also independent of shock-strut extension for small drag loads. This value held for static conditions but would be too high for dynamic conditions.

Dynamic Tests

Level surface drop tests.- The level surface drop tests were conducted at 1.2, 1.5, and 1.8 m/s (4, 5, and 6 ft/s). The primary objectives were (1) to verify computer modeling (ACOLAG) of the gear under dynamic conditions (see appendix A for gear input geometry, etc.); (2) to model the gear accurately without axial friction since ideally no force develops normal to the gear when the gear impacts perpendicular to the level impact surface (the friction force is less than 44 N (10 lbf); and (3) to compare the experimental dynamic tire response with the computer predicted tire response based on the empirical tire force-deflection relation.

Plots of analytical (ACOLAG) and experimental parameter time histories for drop tests onto a level impact surface are presented in figure 6. The tire deflection and shock strut stroke time histories are shown in figures 6(a) and 6(b), respectively, and are given, for convenience, a positive sign. Figures 6(c) and 6(d) show the hydraulic and pneumatic pressure differentials above the fully extended gear charging pressure. (Pressure of 0 in figs. 6(c) and 6(d) corresponds to a charging pressure of 1917 kPa (278 psig).) The hub and upper mass acceleration time histories in g units are presented in figures 6(e) and 6(f), respectively. The analytical values predicted by ACOLAG (solid lines) can be directly compared to the experimental points in all plots (figs. 6(a) to 6(f) for the 1.2-, 1.5-, and 1.8-m/s (4-, 5-, and 6-ft/s) drops). The computer program began computation with time 0 at honeycomb contact with the initial velocity and the initial tire height above the impact surface specified. For convenience in comparing tests of differing velocities, however, all plots are shown with time 0 adjusted to the time of tire contact.

A comparison of computer predictions with the experimental data in figure 6(a) indicates that overall tire deflection was predicted well. Some discrepancy does exist beyond 0.08 s, especially at 1.8 m/s (6 ft/s), and may be explained as tire hysteresis effects (not modeled in the computer program) for the unloading tire. Even without hysteresis effects, the empirical tire relation (which agrees well with the pseudostatic values) is also satisfactory under dynamic conditions.

The shock strut stroke (fig. 6(b)) varied from 5.6 cm (2.2 in.) for the 1.2-m/s (4-ft/s) impact velocity to 11.2 cm (4.4 in.) for the 1.8-m/s (6-ft/s) impact velocity.

The static stroke for the gear supporting the drop mass was 14.6 cm (5.8 in.). The stroke for all three impacts did not reach this static condition because of the lift simulation technique.

In figure 6(c), the experimental hydraulic pressure data compare well with the analytical curves for all velocities, except for the shape of the peaks. Tire hysteresis probably contributes to the deviation between the experimental and analytical pressure for the time interval 0.06 to 0.10 s since the analytical model neglects hysteresis effects. The strut pneumatic pressure shown in figure 6(d) agrees very well with the analytical curves since it is primarily a function of shock strut stroke which was modeled quite accurately. A comparison of the curves in figures 6(c) and 6(d) indicates that the hydraulic and pneumatic pressures equalize shortly after impact.

The hub acceleration (fig. 6(e)) is delayed until the tire force builds to a value greater than the gear pneumatic charging force plus the friction force, after which the hub rapidly accelerates. Before shock strut stroking, the gear and the upper mass move dynamically as a rigid body with the same acceleration. The maximum upper mass acceleration, shown in figure 6(f), which occurs for the 1.8-m/s (6-ft/s) case does not exceed -1.6g, while the hub with its low mass (fig. 6(e)) experiences much higher accelerations. The initiation of shock strut stroking is noticeable analytically in figure 6(f). The time of honeycomb rebound can also be determined from figure 6(f). For the 1.2-m/s (4-ft/s) drop, the rebound occurs at 0.15 s, and the acceleration decreases to 0g and actually becomes positive as the upper mass leaves the honeycomb. The honeycomb begins reloading around 0.22 s and again unloads at approximately 0.24 s. The rebound of the mass from the honeycomb (bounce) is evident on the oscillograph record as a series of pulses with decaying amplitude occurring at nearly regular intervals. Only one bounce is shown in figure 6(f) for the 1.2-m/s (4-ft/s) case. At 1.8 m/s (6 ft/s), however, the first bounce cannot be seen since it occurs beyond 0.28 s. The honeycomb bounce is duplicated analytically to a high degree of accuracy in both frequency and magnitude.

For all of the six parameters measured in the drop tests on the level surface, overall experimental-analytical agreement was excellent. Such agreement provided confidence in the analytical model and in the empirical tire force-deflection equation.

Inclined surface drop tests.- Tests at 1.5 m/s (5 ft/s) on inclined surfaces were conducted to determine the dynamic effects of internal friction and strut fore-and-aft bending. To study the effects of axial friction, the level surface of the previous tests was replaced with surfaces inclined at 5° and 10°. Inclined surfaces were used rather than an inclined gear and level impact surface. To prevent possible damage to the gear, 10° was chosen as the largest angle of inclination. In an actual landing with an inclined gear, the drag moment and the tire force moment oppose each other, but in the experimental vertical drop tests only one significant moment develops. Calculations indicated

that the maximum normal force to the gear at the hub would probably exceed 2.67 kN (600 lbf) for impacts on the 10° surface.

Experimental and analytical data for impacts on the 0°, 5°, and 10° surfaces are shown in figure 7. The time histories in figure 7 are ordered as in figure 6 with figures 7(a) and 7(b) showing the tire deflection and shock strut strokes, figures 7(c) and 7(d) showing the hydraulic and pneumatic pressures, and figures 7(e) and 7(f) showing the hub and upper mass accelerations. Analytical data were obtained for the 5° and 10° inclined surface tests with the friction coefficient varied from 0.05 to 0.25. A friction coefficient of 0.15 gave the best overall fit to the experimental data shown in figure 7 when all parameters were considered. This value is considerably lower than the 0.27 value obtained from the pseudostatic tests (appendix B). The strut bending and the oscillation set up in the 10° test were more severe than had been anticipated. The analytical simulation of the hub accelerations (which did not include strut bending effects) with a constant friction coefficient is a faired fit and does not follow the detailed oscillations.

The peak tire deflection (fig. 7(a)) varies approximately from 4.6 cm (1.8 in.) for the 5° test to approximately 5.2 cm (2.05 in.) for the test with the 10° inclined surface. Peak deflections are predicted well analytically, but again deviations are thought to result from tire hysteresis and effects associated with strut bending.

A comparison of the shock strut stroke for the different impact surfaces is given in figure 7(b). Experimentally, the maximum stroking distance for drops on the level, 5°, and 10° surfaces are approximately 9.4 cm (3.7 in.), 8.4 cm (3.3 in.), and 7.1 cm (2.8 in.), respectively. Analytically, the stroke calculated using a constant 0.15 friction coefficient agrees well with the experimental data for the tests on the 5° inclined surface. At first, with the 0.15 friction coefficient analytical and experimental data agree quite well for drops for the surface inclined 10°, but agreement lessens after 0.10 s because of strut bending effects.

The hydraulic pressure time history shown in figure 7(c) shows good analytical and experimental agreement for the 0° and 5° impact tests. However, for tests on the 10° inclined surface, a large oscillation in the experimental data, thought to arise primarily from strut bending, was not modeled analytically. Again, the pneumatic pressure curves in figure 7(d) reflect the accuracy of the shock strut stroke since pneumatic pressure is a function of volume change or strut stroke.

Not surprisingly, the hub acceleration with its small mass proved to be very sensitive to axial friction. In figure 7(e), the main peak at approximately 0.025 s is predicted fairly well in both shape and magnitude for all tests. The large oscillations in the hub acceleration for tests on both the 5° and 10° inclined surfaces were very repeatable. These oscillations occurred at a frequency of approximately 23 Hz. This oscillation can

be traced to the fore-and-aft bending of the gear at its fundamental frequency by using the pseudostatic spring constant data from figure 8. Figure 7(e) shows that the center of an oscillation for the 10^{o} test occurs at 0.10 s after tire contact. The shock strut stroke at this time (fig. 7(b)) is approximately 6.4 cm (2.5 in.) which with a total available stroke of 22.9 cm (9.0 in.), corresponds to 72-percent extension. In figure 8 the spring constant corresponding to this extension is 401 kN/m (27 500 lbf/ft). The calculated frequency for this spring constant with the hub mass of 25.3 kg (55.7 lbm) is 20.0 Hz, nearly the same as the observed frequency of the hub acceleration around 0.10 s. Consequently, under extreme conditions, the fore-and-aft bending of the gear can have a large effect on the gear axial friction and on the gear dynamics.

CONCLUDING REMARKS

Results of this investigation define some critical landing gear characteristics required for the accurate dynamic simulation of a light aircraft landing gear and provide verification of the analytical model. Pseudostatic tests determined that the maximum brake torque as a function of brake pressure was approximately linear with a slope of 0.00023 N-m/Pa (1.18 lbf-ft/psi) over the range investigated. The strut fore-and-aft spring constant varied linearly from 342 kN/m (23 400 lbf/ft) for 90-percent extension to 644 kN/m (44 100 lbf/ft) for 10-percent shock strut extension. The gear axial static friction coefficient for the pseudostatic tests was approximately 0.27 and independent of shock strut extension for small drag loads. Experimental pseudostatic tire force-deflection characteristics compared very well with the empirical predictions.

Level surface drop tests with honeycomb lift simulation at impact velocities of 1.2, 1.5, and 1.8 m/s (4, 5, and 6 ft/s) were modeled with computer program active control landing gear analysis (ACOLAG) with excellent agreement for all measured parameters which included tire deflection, shock strut stroke, pneumatic pressure, hydraulic pressure, hub acceleration, and upper mass acceleration. Honeycomb lift simulation was found to be accurate and reliable although representative of only the impact phase of the landing. The experimental tire response compared very well with the computer predicted tire response which was based on an empirical tire force-deflection relation. Some discrepancy in the analytical tire response was noted and was thought to result from hysteresis effects which were not modeled.

Drop tests at an impact velocity of 1.5 m/s (5 ft/s) onto surfaces inclined at 5^{o} and 10^{o} to the horizontal were modeled with computer program ACOLAG to determine the average dynamic axial-friction coefficient. A value of 0.15 gave the best overall computer fit to the experimental data and was considerably smaller than the value obtained from the pseudostatic data. Strut bending and associated axial binding for the 10^{o} inclined surface drop tests were more severe than had been anticipated. Experimentally, the vertical hub

acceleration displayed a large oscillation of approximately 23 Hz occurring after the main impact peak. This oscillation corresponds well with the natural fore-and-aft bending frequency of the gear as calculated from the experimentally determined pseudostatic spring constant. Consequently, under extreme conditions the fore-and-aft bending of the gear can have a large effect on the gear axial friction and on the gear dynamics.

Langley Research Center
National Aeronautics and Space Administration
Hampton, VA 23665
August 26, 1977

APPENDIX A

DESCRIPTION OF LANDING GEAR

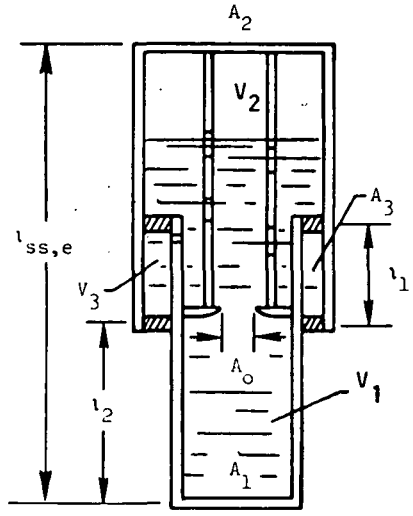

Sketch (a)

The important geometric characteristics of the landing-gear shock strut are illustrated in sketch (a). The computer program input parameters follow:

Shock strut:

Pneumatic area, A_2, m^2 (ft^2)	0.00535	(0.05754)
Hydraulic area, A_1, m^2 (ft^2)	0.00317	(0.03409)
Primary orifice area, A_0, m^2 (ft^2)	0.00008	(0.00085)
Fluid volume in piston below orifice plate, V_1 (gear extended), m^3 (ft^3)	0.00074	(0.0260)
Pressurized pneumatic volume, V_2 (gear extended), m^3 (ft^3)	0.00122	(0.0432)
Volume between cylinder and piston, V_3 (gear extended), m^3 (ft^3)	0.00011	(0.0040)
Charging pressure, $p_{o,a}$, kPa (psfg)	1850.2	(38 643)
Bearing separation for fully extended shock strut, l_1, m (ft)	0.1544	(0.5065)
Axial length from hub to lower bearing for fully extended shock strut, l_2, m (ft)	0.6727	(2.2071)
Drop mass (mass acting on gear), kg (lbm)	1490	(3280)
Hub mass (wheel, tire, and piston), kg (lbm)	25.3	(55.7)
Maximum shock strut stroke, m (ft)	0.229	(0.75)
Fully extended length of shock strut, $l_{ss,e}$, m (ft)	1.1135	(3.65334)
Area between piston and cylinder, A_3, m^2 (ft^2)	0.00151	(0.01626)

Specific weight of hydraulic fluid, γ_H, N/m^3 (lbf/ft^3)	8226	(52.36)
Dynamic viscosity of hydraulic fluid, μ_H, N-sec/m^2 (lbf-sec/ft^2)	0.00862	(0.00018)
Mass density of hydraulic fluid, ρ_H, kg/m^3 (slugs/ft^3)	838	(1.626)
Volume of hydraulic fluid, V_H, m^3 (ft^3)	0.00164	(0.05801)

Wheel and tire:

Wheel flange diameter, m (ft)	0.2954	(0.9692)
Unloaded diameter of tire, d, m (ft)	0.552	(1.81)
Maximum width of undeflected tire, w, m (ft)	0.175	(0.5735)
Unloaded rated inflation tire pressure, p_r, kPa (psf)	55.16	(1152)
Unloaded tire inflation pressure, p_o, kPa (psf)	413.7	(8640)
Pressure rise parameter, κ	0.62	
Vertical force coefficient, C_Z	0.03	

APPENDIX B

APPARATUS, TEST SETUP, AND PROCEDURE FOR PSEUDOSTATIC TESTS

Gear Fore-and-Aft Spring Constant

The basic configuration of the gear with mounting fixture for both the fore-and-aft spring constant and axial-friction tests is shown in figure 12. In order to compute the spring constant, the gear was mounted horizontally as a cantilever and tip drag loads were applied for 10-, 50-, and 90-percent extensions of the shock strut. Maximum tip load ranged from 3.56 kN (800 lbf) for 90-percent shock strut extension to 6.23 kN (1400 lbf) for a 10-percent extension. Deflections were measured with a sensitive dial gauge indicator. The relation between drag load and gear bending deflection for the three shock strut extensions is plotted in figure 13. Taking the slope of each line allowed derivation of the elastic spring constant for each extension. The three points were plotted on a graph (fig. 8) with spring constant as the ordinate and shock strut extension as the abscissa. The spring constant is seen to vary from 342 kN/m (23 400 lbf/ft) for 90-percent extension of the strut to 644 kN/m (44 100 lbf/ft) for a 10-percent extension. Although the spring constant variation with strut extension is nonlinear, a linear fit can be made to the points with little loss of accuracy.

Brake Torque as a Function of Brake Pressure

The experimental setup to determine maximum brake torque as a function of hydraulic brake pressure is illustrated schematically in figure 14. Instrumentation required for this test consisted of a load cell for measuring applied force (and hence torque) and a mechanical pressure gauge for measuring applied brake pressure. The test procedure was first to apply a known hydraulic brake pressure and then to measure the force level necessary to initiate rotation of the wheel. This force multiplied by the length of the torque arm gave the maximum brake torque for the set hydraulic brake pressure. The procedure was repeated three times for each pressure, and the average values were plotted as shown in figure 9.

Experimental Determination of Tire Force-Deflection Characteristics

The determination of nonrolling tire force-deflection characteristics was accomplished by use of a compression loading machine. The tire (an 8-ply, 6.50-10, type III aircraft tire) and wheel were mounted on the test-fixture axle (fig. 15) which was attached to the upper platen of the testing machine. The tire was loaded to a maximum force of

13.34 kN (3000 lbf) in increments of 0.22 kN (50 lbf) initially and in 1.33-kN (300-lbf) increments after the curve had begun to level off.

The experimental loading and unloading curve and the semiempirical curve (ref. 4)

$$F = 2.4\left[p + \kappa p_{o,a}\left(\frac{\delta}{w}\right)^2 + 0.08p_r\right] w\sqrt{wd}\left\{\frac{\delta}{w} - C_Z\left[1 - e^{\frac{-0.6\left(\frac{\delta}{w}\right)}{C_Z}}\right]\right\}$$

are plotted in figure 10. The above terms are:

F	load, N (lbf)
δ	tire deflection, m (in.)
w	maximum width of undeflected tire, m (in.)
d	unloaded tire diameter, m (in.)
p	absolute tire pressure, Pa (psi)
κ	pressure rise parameter
$p_{o,a}$	initial inflation pressure, Pa (psi)
p_r	rated tire pressure, Pa (psi)
C_Z	vertical force coefficient

As can be seen from figure 10 the agreement is excellent in loading. The loading rate was slow and the deflections were read using a dial gauge. Some tire hysteresis is present in the unloading cycle.

Axial Friction Due to Applied Drag Loads

To determine the axial friction F_f due to applied drag loads, the gear and test fixture were mounted horizontally on a vertical backstop (fig. 12). The gear was drained of hydraulic fluid and the filler plug (with air valve) was removed.

Dead weight drag loads were applied (up to 1.33 kN (300 lbf)) for 10-, 50-, and 90-percent extensions of the shock strut. An external hydraulic cylinder was used to

initiate axial motion, and the force necessary was read using a load cell. The axial motion was limited to approximately 2.5 cm (1.0 in.); the motion took place in most cases at a very slow rate. The friction obtained by this method was probably static, not kinetic, because the motion was abrupt and jerky instead of smooth and continuous.

Equilibrium of vertical forces on the lower mass (piston and hub) gives the normal force on the lower bearing N_2

$$N_2 = N_1 + W + D \tag{B1}$$

where

N_1 normal force on upper bearing

W weight of lower mass (hub plus steel test cylinder); total 0.18 kN (40 lbf)

D applied load on lower mass (drag load)

Equilibrium of moments about the lower bearing is used to give the upper bearing normal force

$$N_1 = \frac{W\,\ell_W + D\,\ell_D}{\ell_1} \tag{B2}$$

with

ℓ_D distance from lower bearing to point of external load application

ℓ_W distance from lower bearing to center of gravity of lower mass

ℓ_1 distance from lower bearing to upper bearing

Finally if the friction coefficient C_f is the same for both bearing surfaces, then F_f, the shock strut axial-friction force, is

$$F_f = C_f\left[W\left(\frac{2\ell_W}{\ell_1} + 1\right) + D\left(\frac{2\ell_D}{\ell_1} + 1\right)\right] \tag{B3}$$

The experimental axial-friction force as a function of drag load D is shown in figure 11 for 10-, 50-, and 90-percent extension of the shock strut. The analytical curve can be calculated from equation (B3) with a constant friction coefficient of 0.27. This value gives the best average fit to the experimental data. Values used in the equation were measured values and are given in table I.

REFERENCES

1. DC-10 Landing Gear Modified. Aviat. Week & Space Technol., vol. 98, no. 12, Mar. 19, 1973, p. 181.

2. Ropelewski, Robert R.: Airbus Test Tempo Quickening. Aviat. Week & Space Technol., vol. 98, no. 10, Mar. 5, 1973, pp. 32-35.

3. McGehee, John R.; and Carden, Huey D.: A Mathematical Model of an Active Control Landing Gear for Load Control During Impact and Roll-Out. NASA TN D-8080, 1976.

4. Smiley, Robert F.; and Horne, Walter B.: Mechanical Properties of Pneumatic Tires With Special Reference to Modern Aircraft Tires. NASA TR R-64, 1960. (Supersedes NACA TN 4170.)

5. Milwitzky, Benjamin; and Lindquist, Dean C.: Evaluation of the Reduced-Mass Method of Representing Wing-Lift Effects in Free-Fall Drop Tests of Landing Gears. NACA TN 2400, 1951.

6. Westfall, John R.; Milwitzky, Benjamin; Silsby, Norman S.; and Dreher, Robert C.: Summary of Ground-Loads Statistics. NACA TN 4008, 1957.

TABLE I.- DISTANCES USED TO DETERMINE STRUT AXIAL-FRICTION COEFFICIENT

Shock strut extension, percent	Stroke		ℓ_1		ℓ_w		ℓ_D	
	cm	in.	cm	in.	cm	in.	cm	in.
10	20.57	8.1	36.04	14.19	27.64	10.88	46.69	18.38
50	11.43	4.5	27.15	10.69	36.53	14.38	55.58	21.88
90	2.29	.9	17.78	7.00	45.87	18.06	64.92	25.56

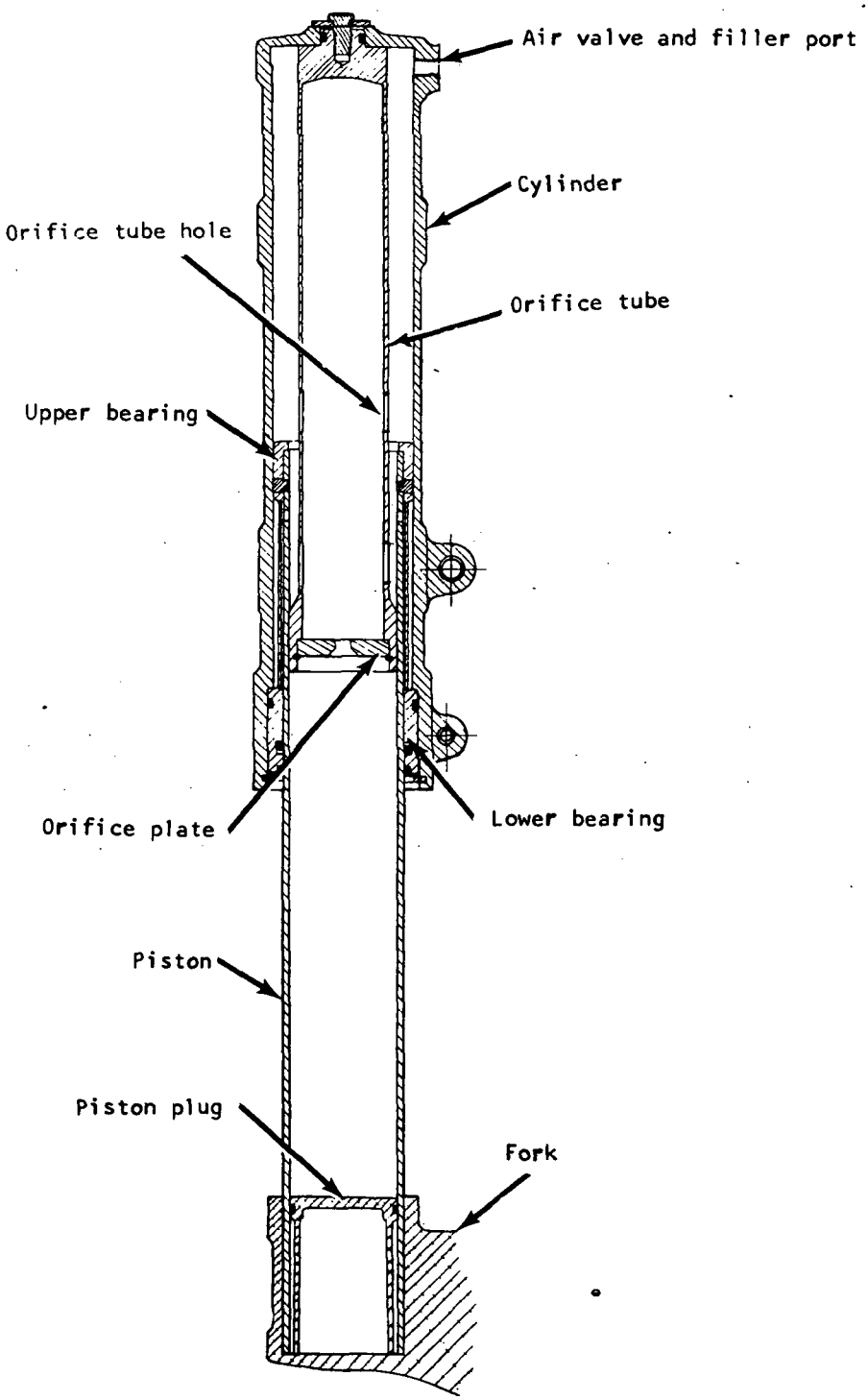

Figure 1.- Internal view of landing gear.

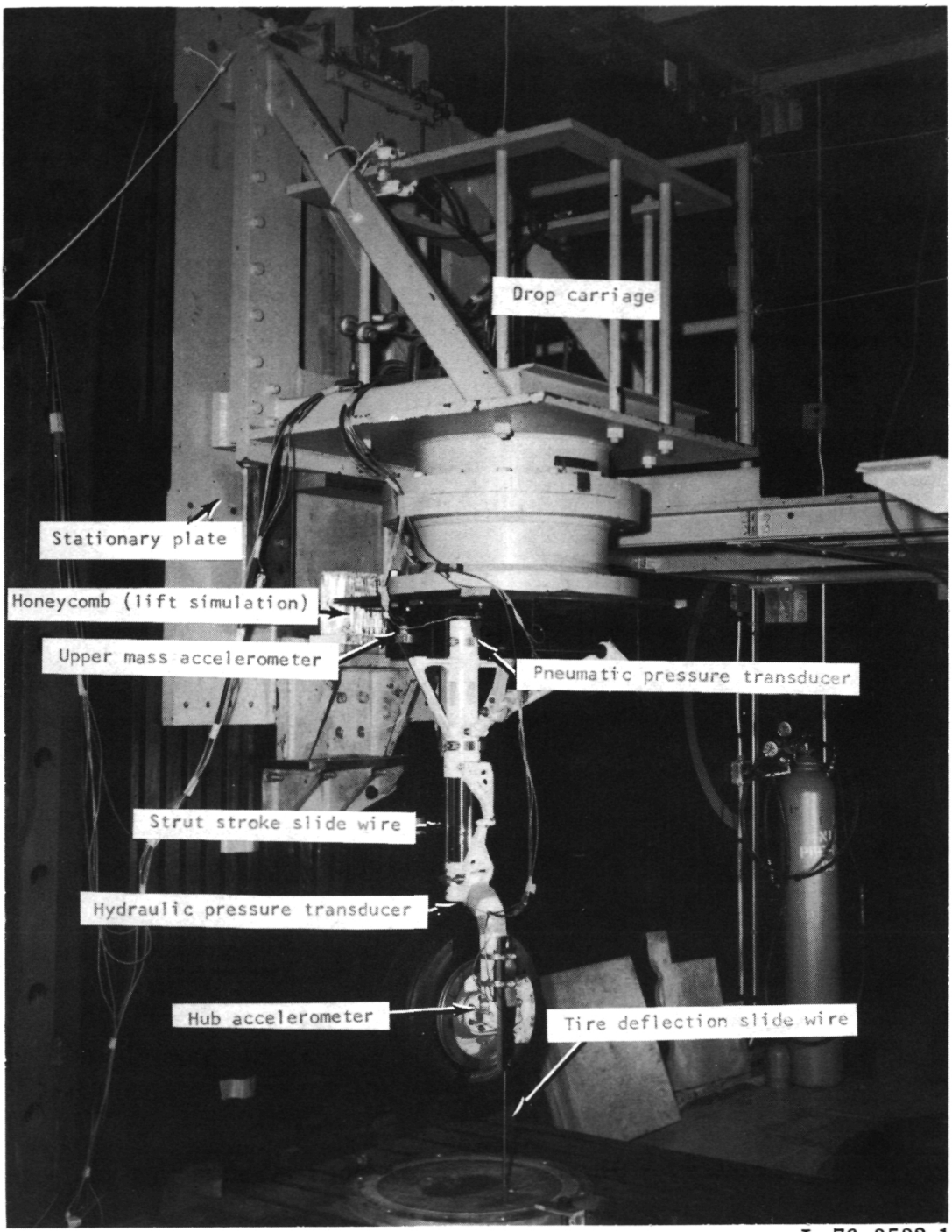

L-76-3532.1

Figure 2.- Dynamic drop test setup.

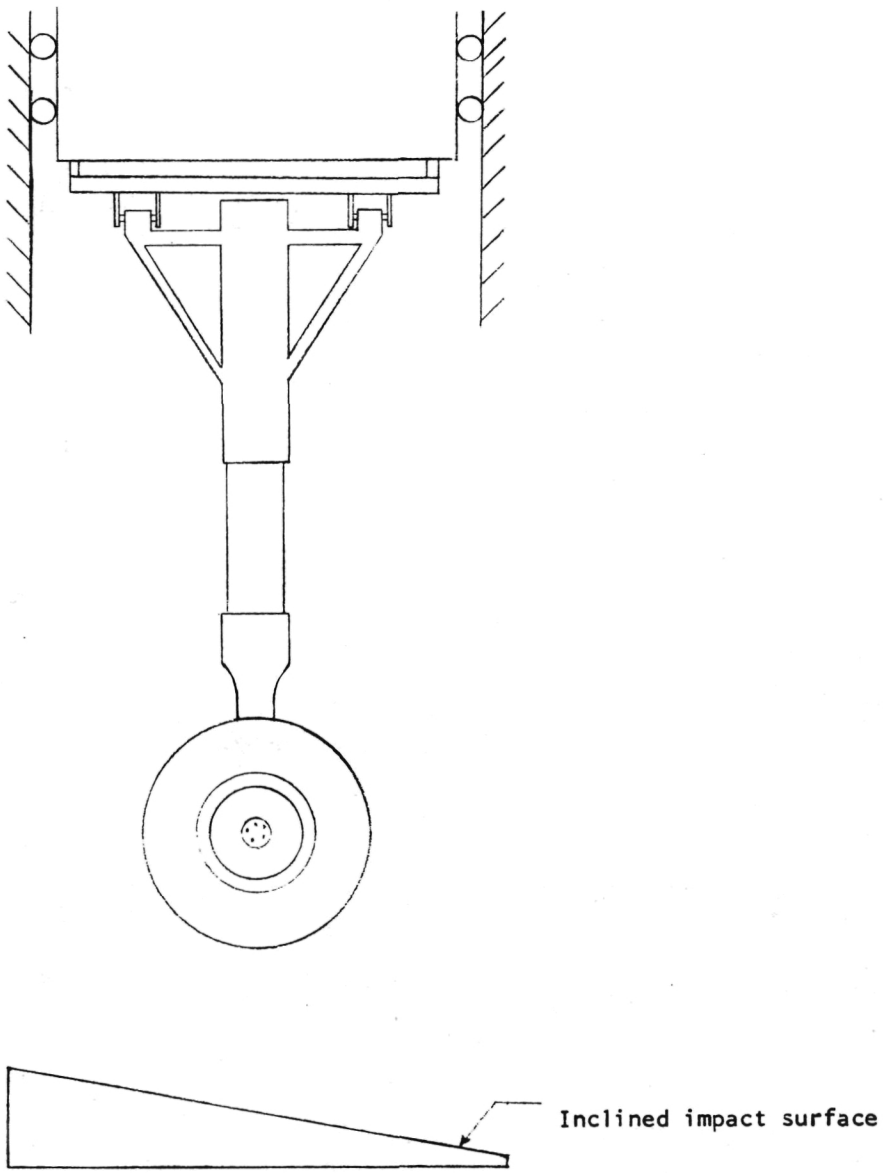

Figure 3.- Drawing of dynamic drop test setup
for inclined surfaces.

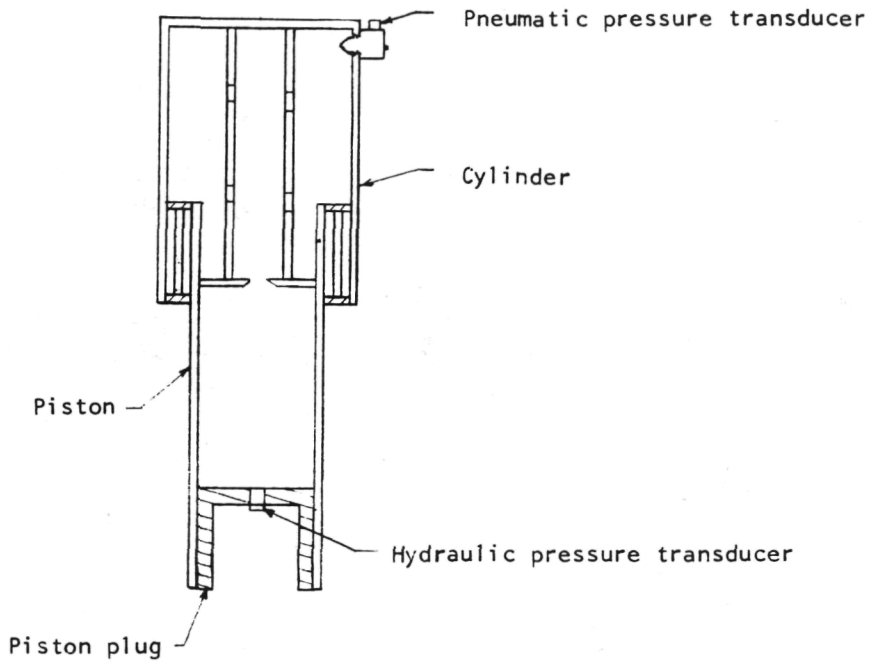

Figure 4.- Location of hydraulic and pneumatic pressure transducers.

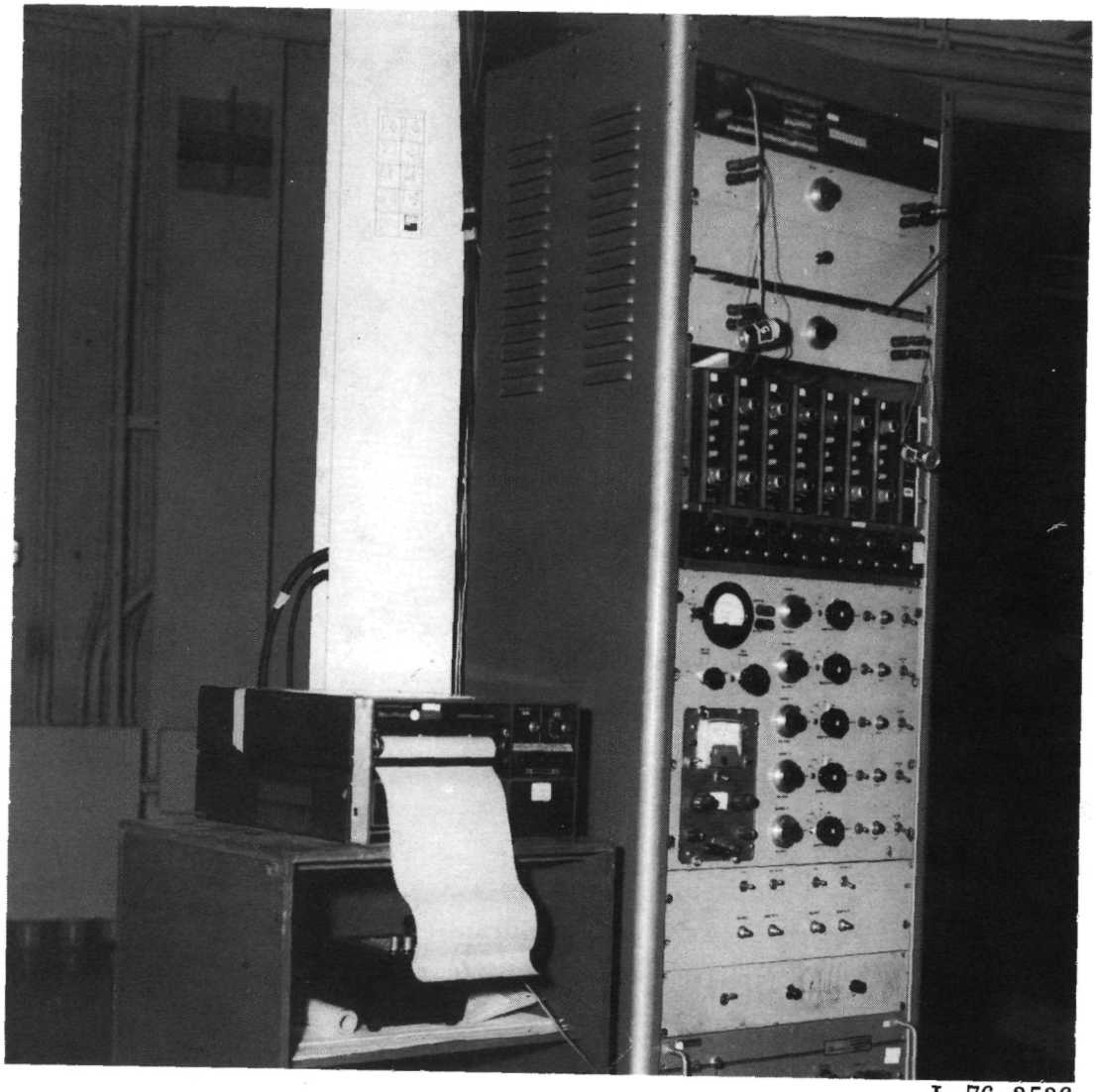

L-76-3536

Figure 5.- Instrumentation rack and oscillograph.

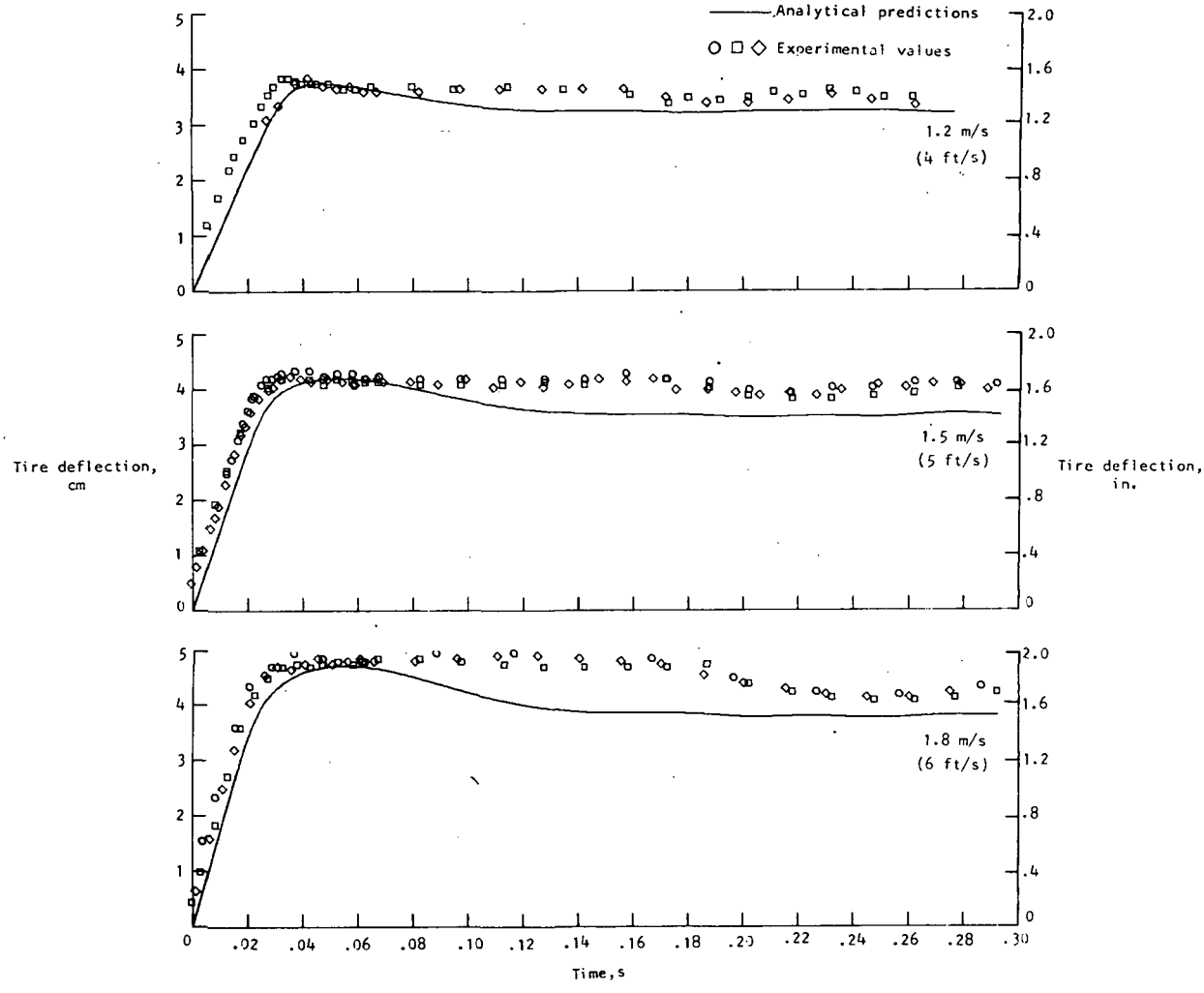

(a) Tire deflection.

Figure 6.- Parameter time histories for drop tests (three runs per test) onto level impact surface.

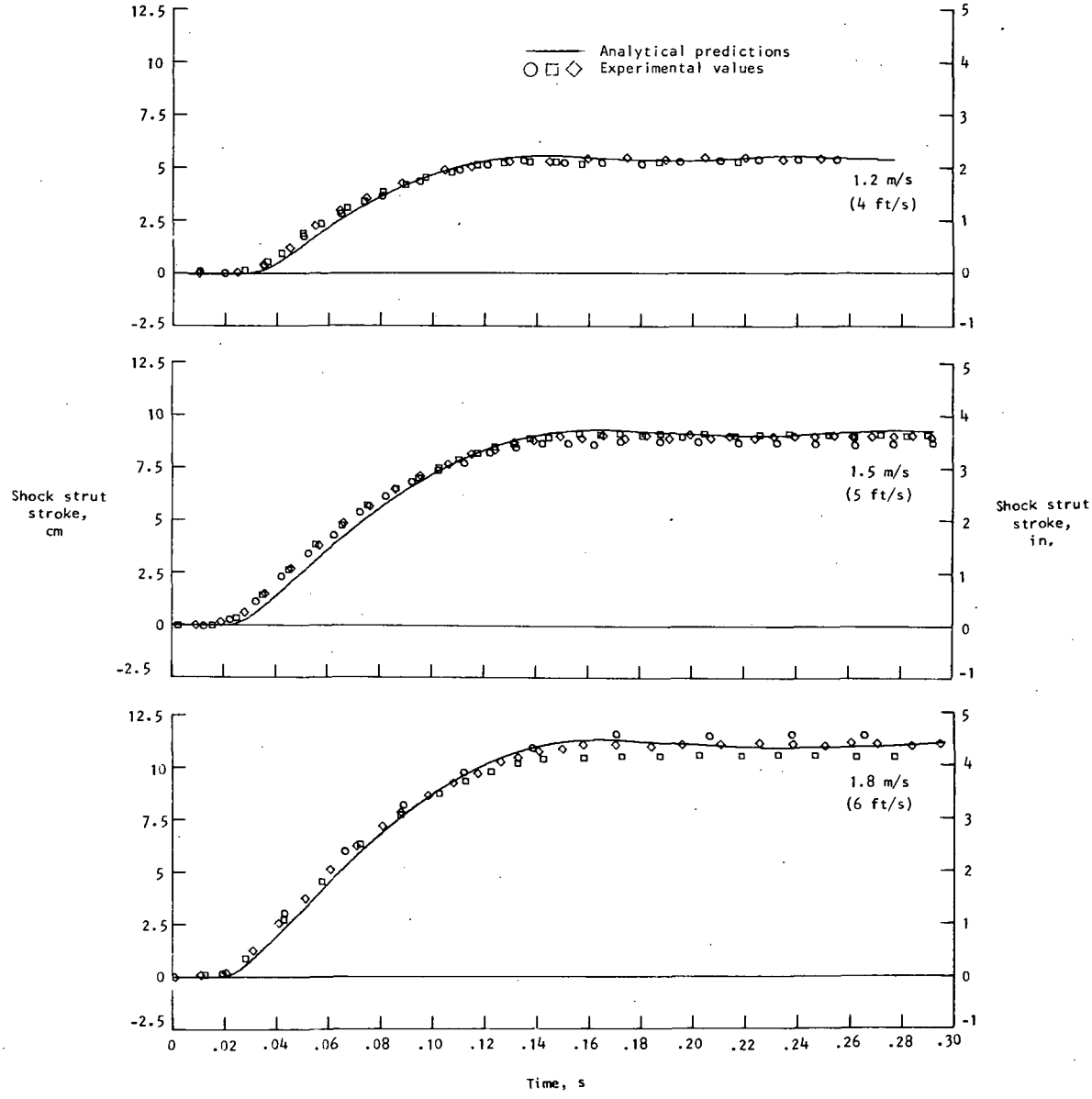

(b) Shock strut stroke.

Figure 6.- Continued.

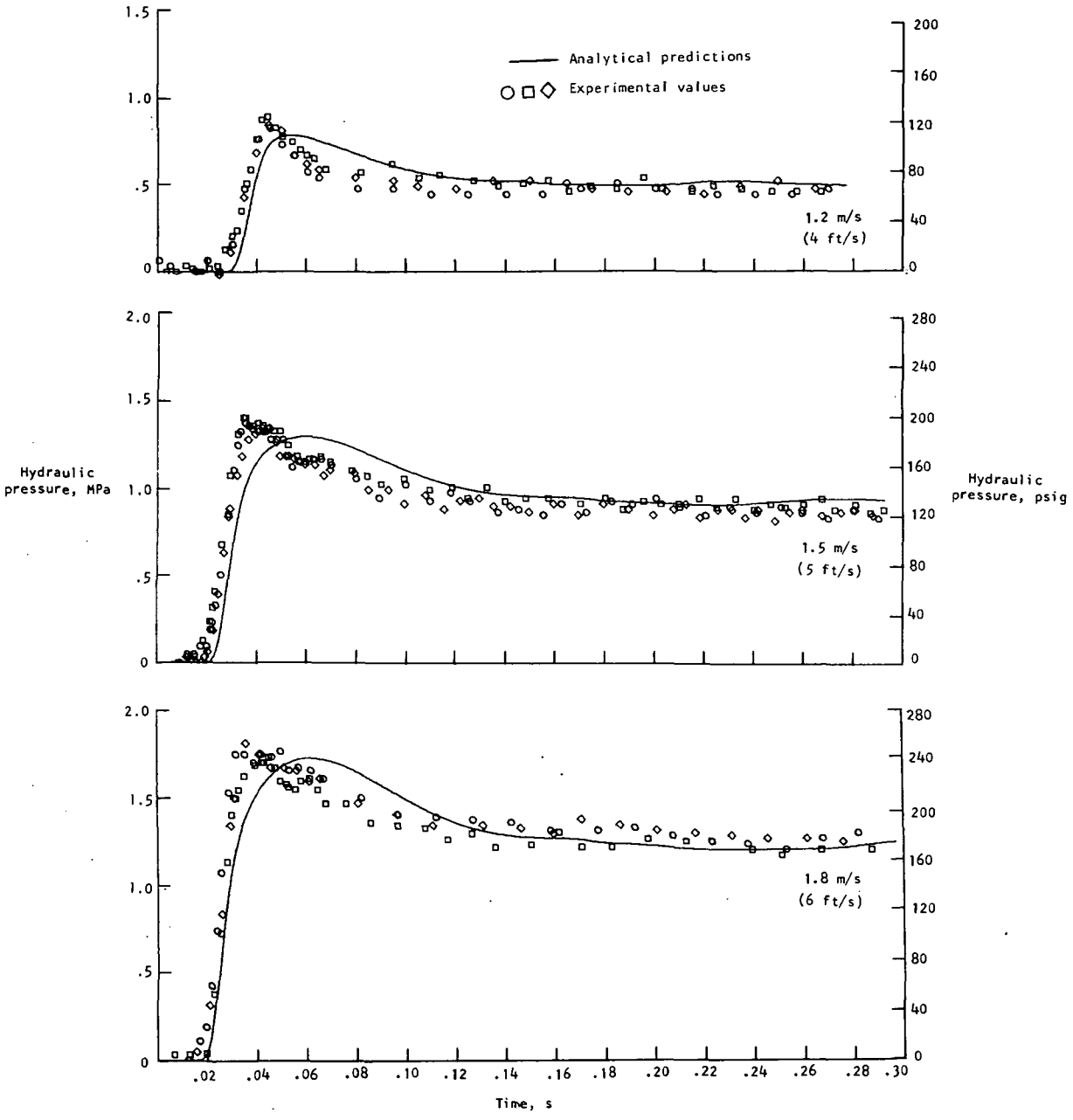

(c) Hydraulic pressure.

Figure 6.- Continued.

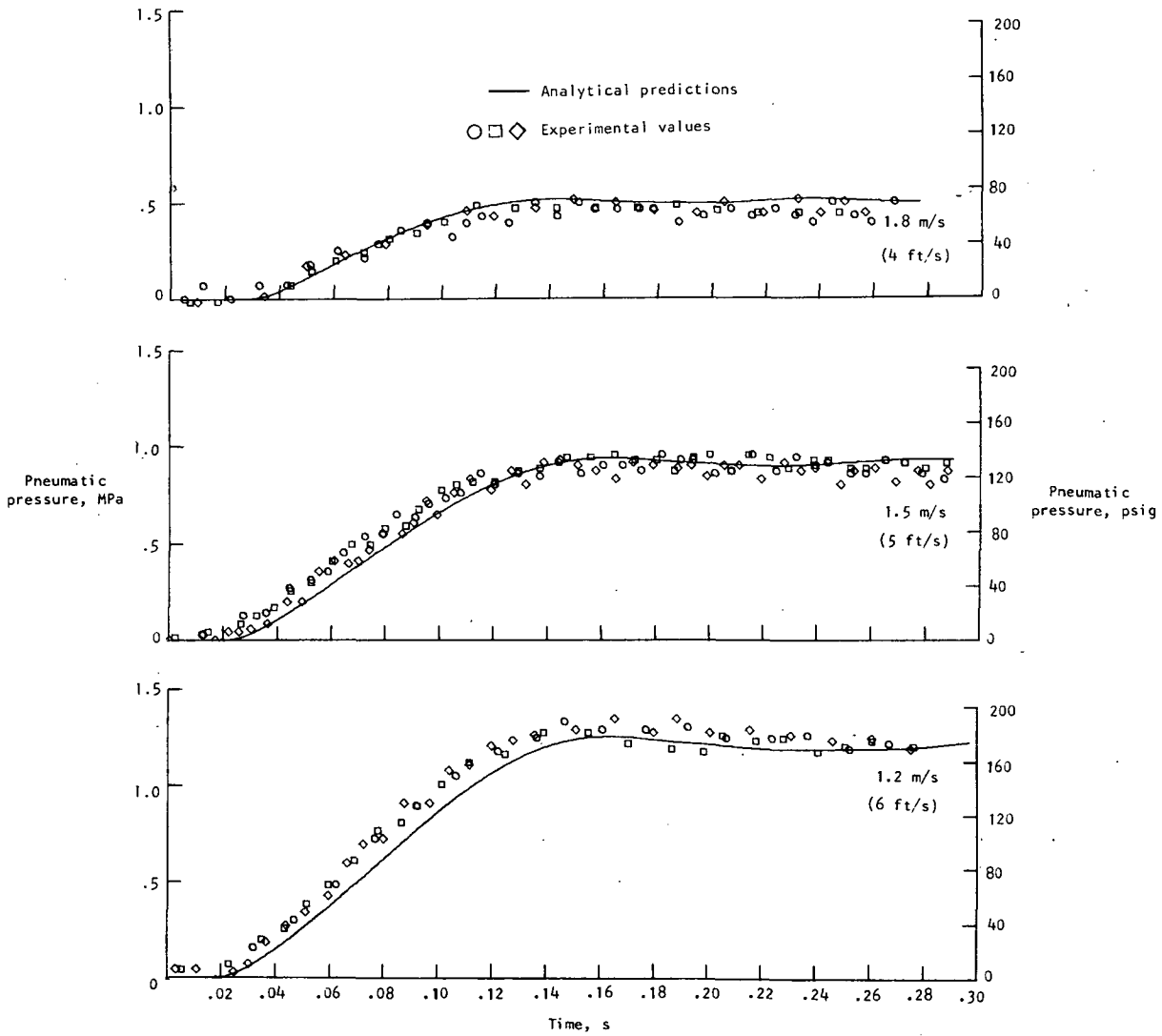

(d) Pneumatic pressure.

Figure 6.- Continued.

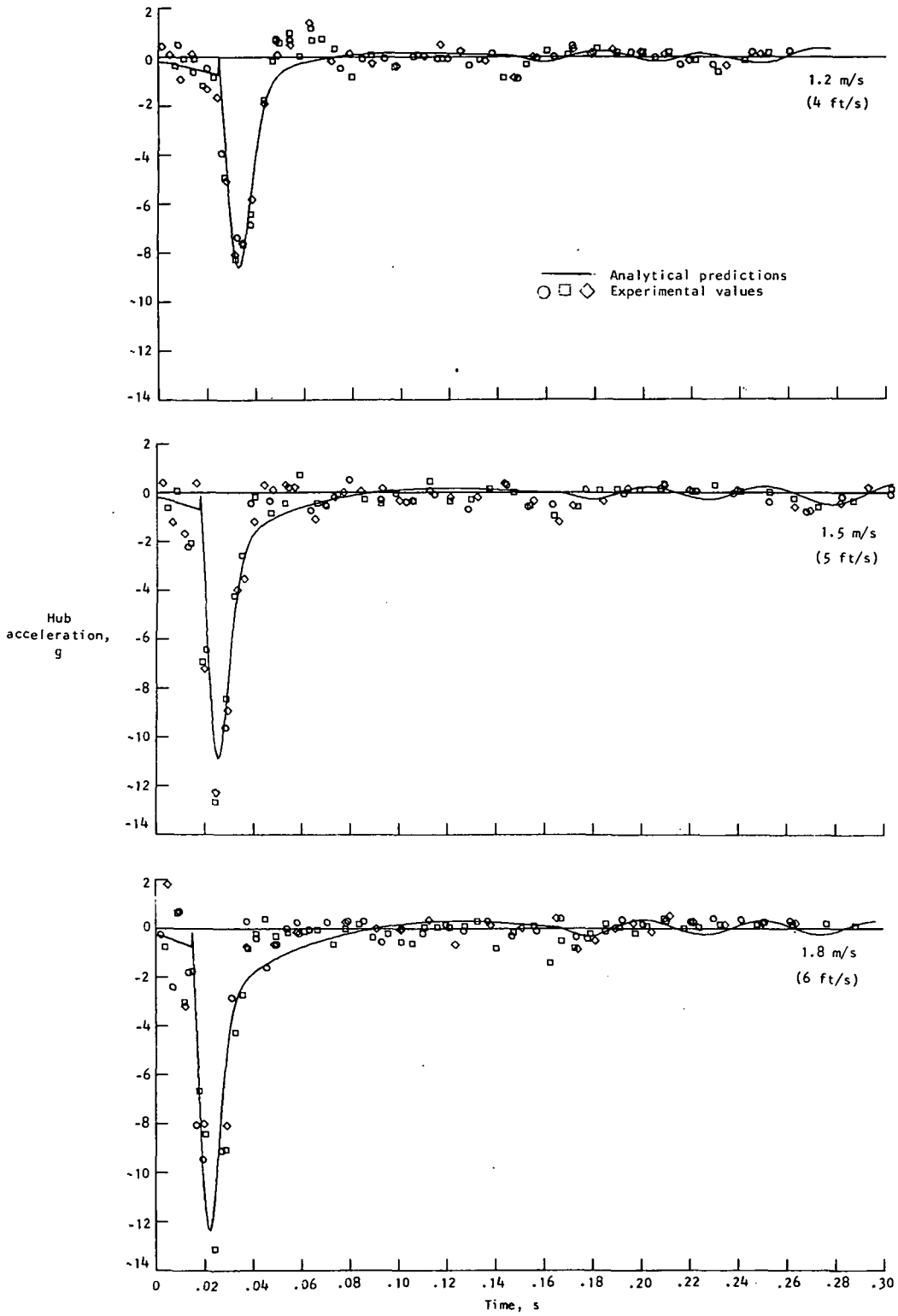

(e) Hub acceleration.

Figure 6.- Continued.

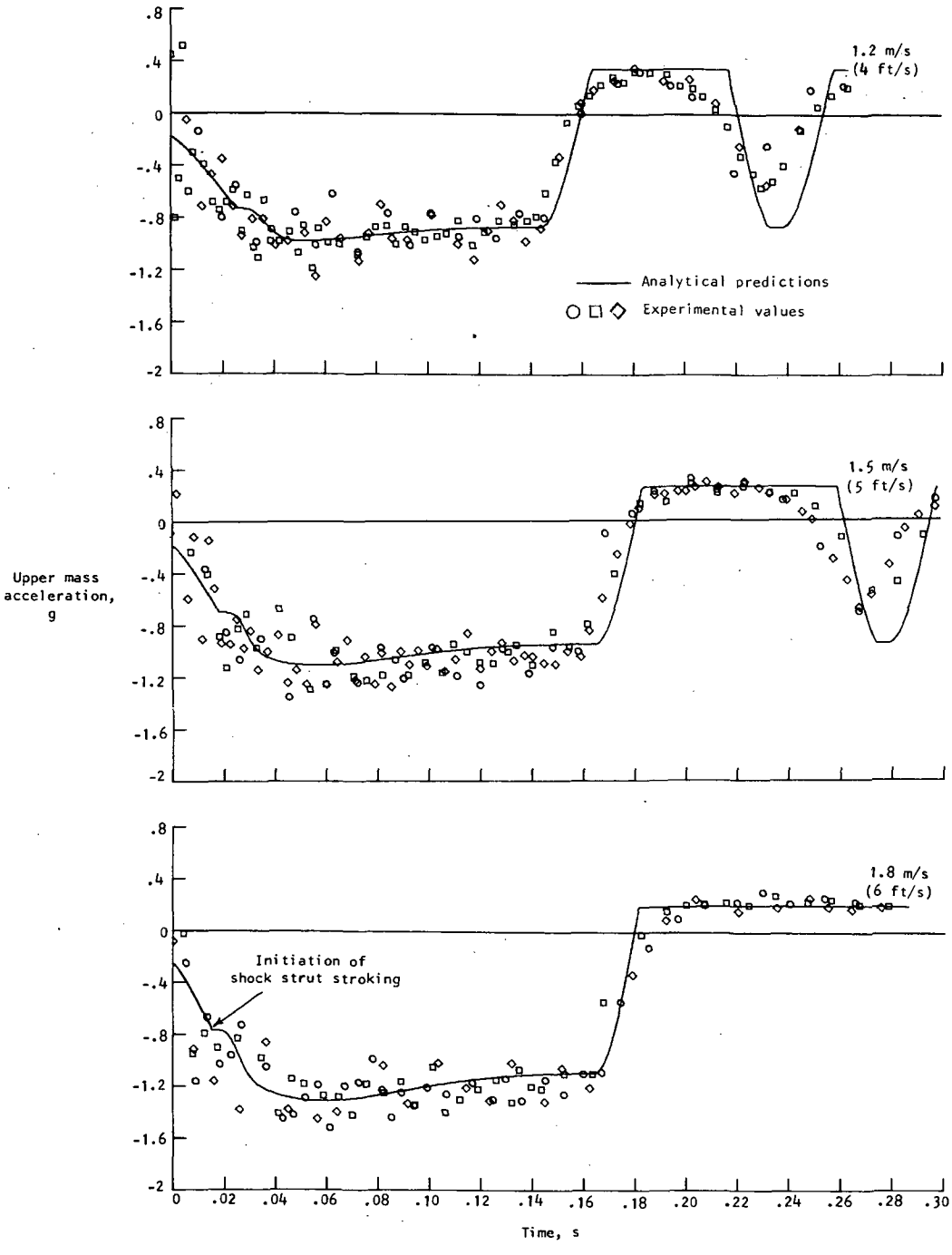

(f) Upper mass acceleration.

Figure 6.- Concluded.

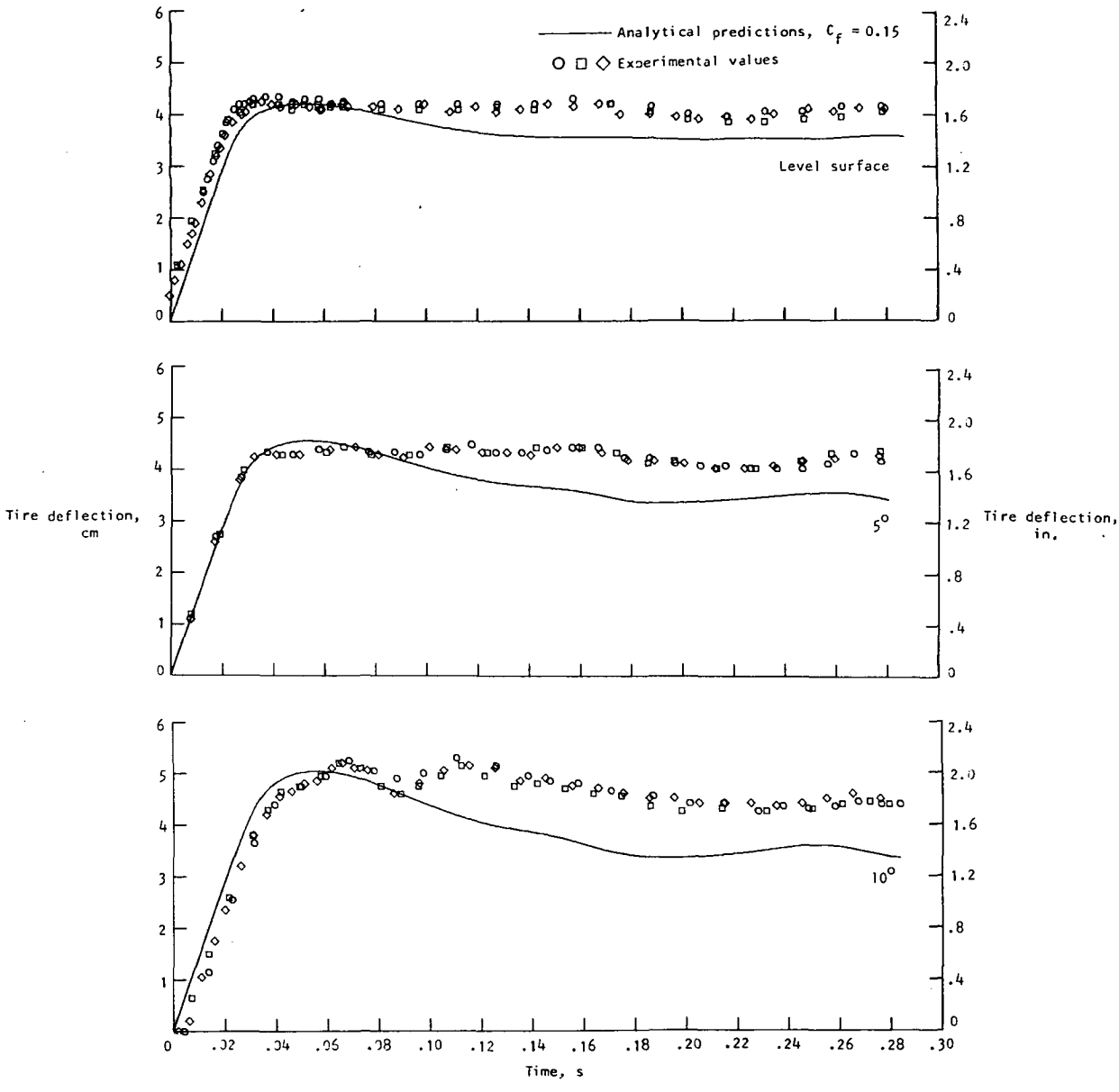

(a) Tire deflection.

Figure 7.- Parameter time histories for drops at 1.5 m/s (5 ft/s) onto 0^o, 5^o, and 10^o inclined surfaces. C_f is bearing friction coefficient.

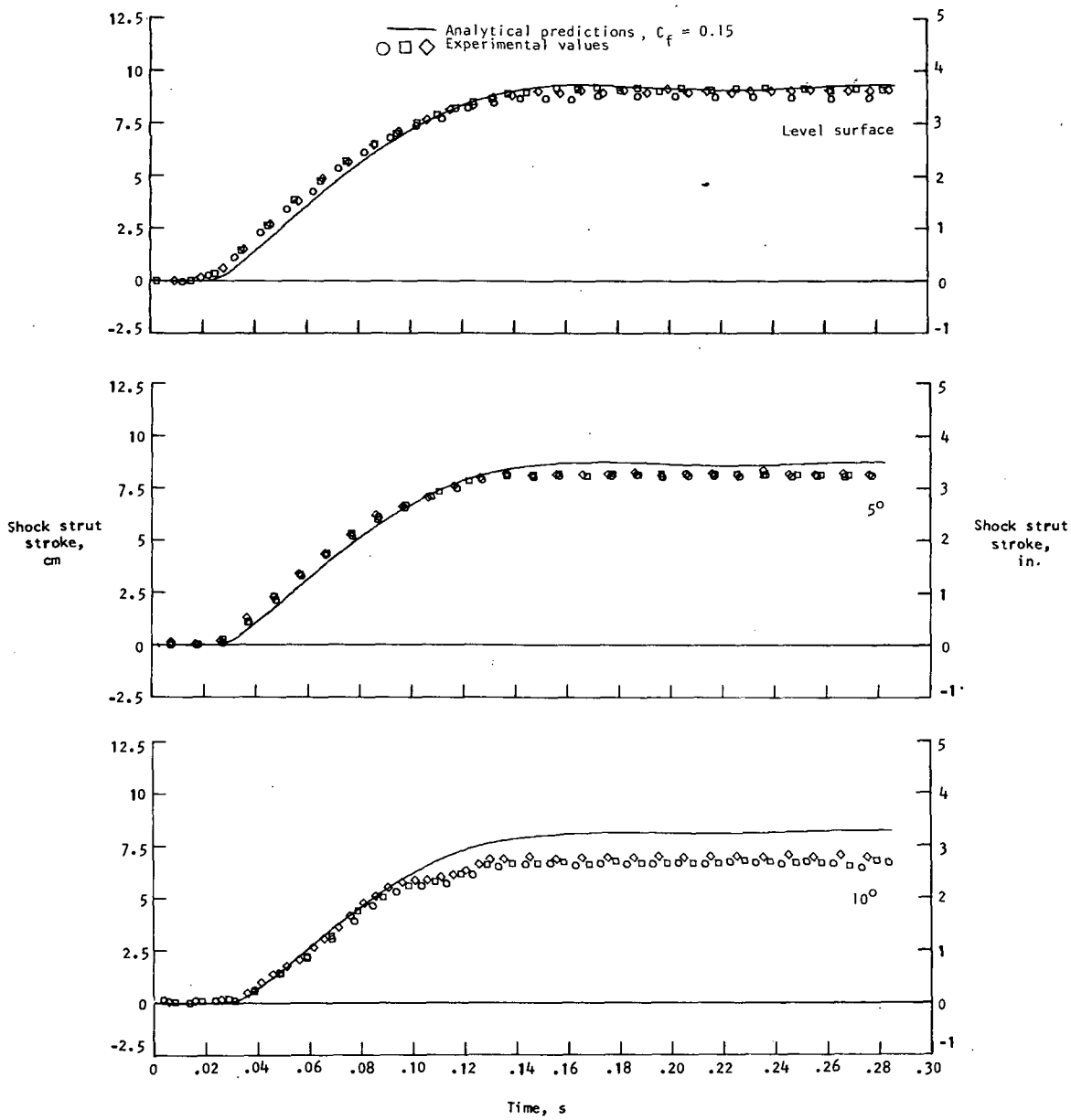

(b) Shock strut stroke.

Figure 7.- Continued.

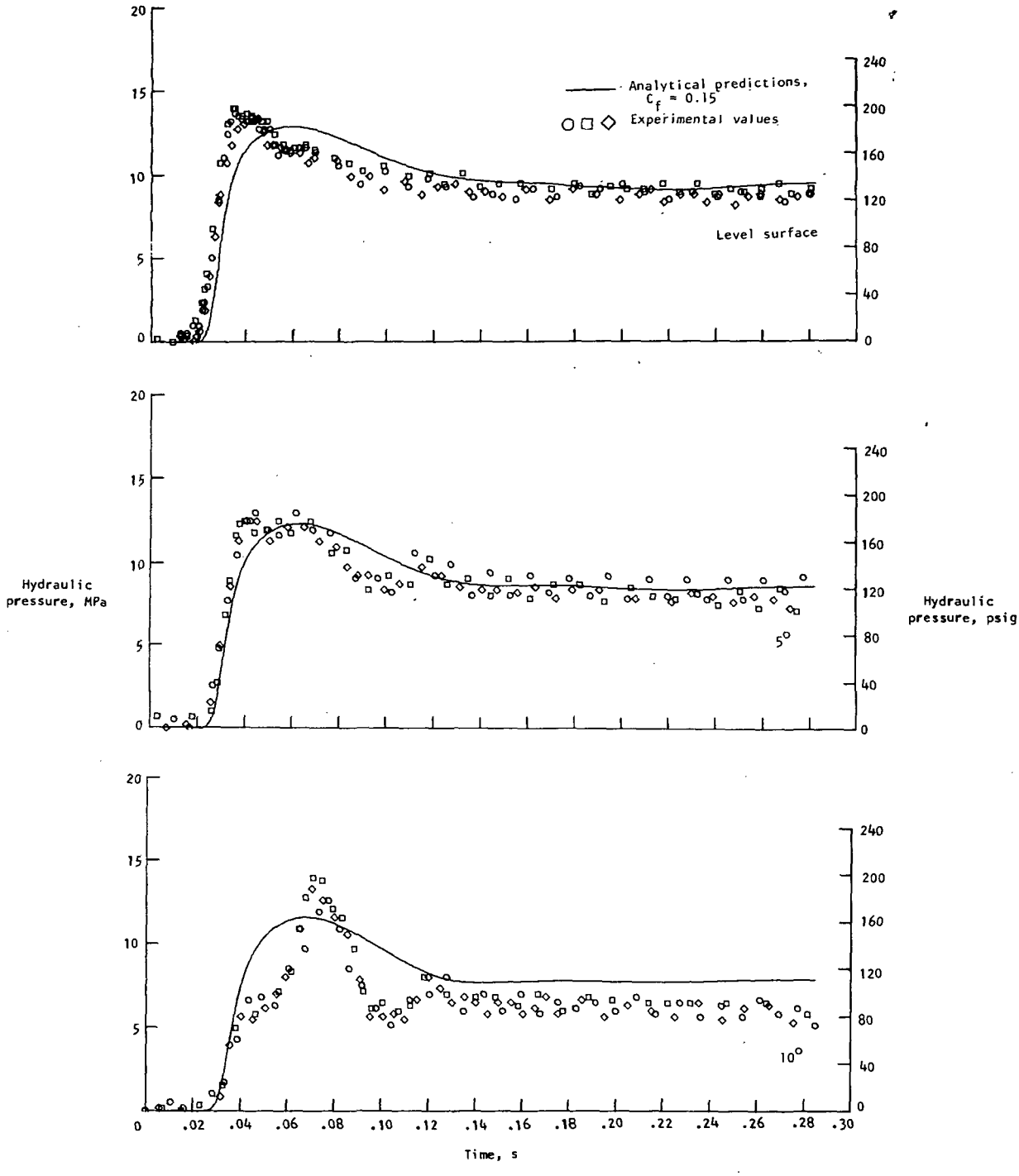

(c) Hydraulic pressure.

Figure 7.- Continued.

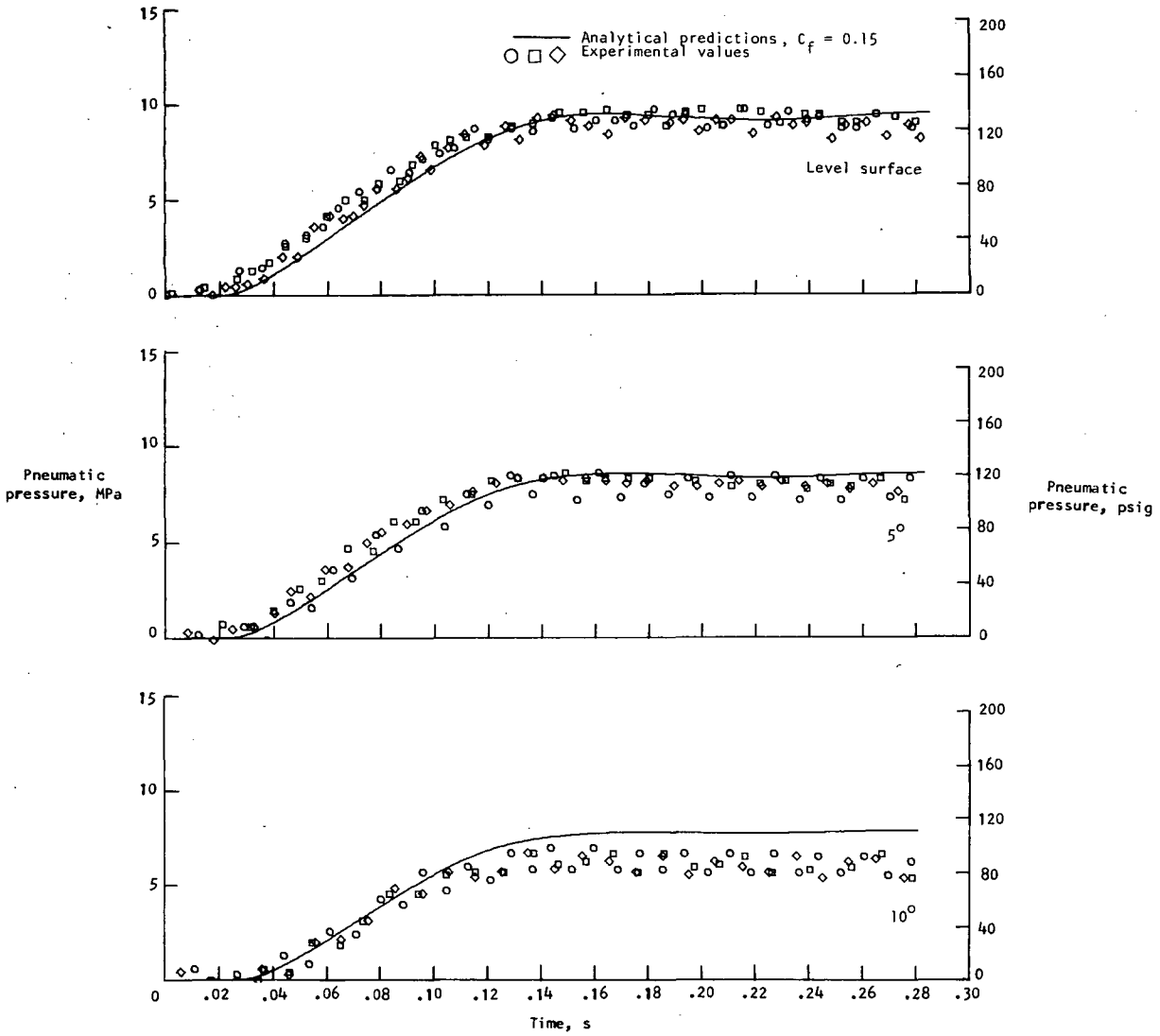

(d) Pneumatic pressure.

Figure 7.- Continued.

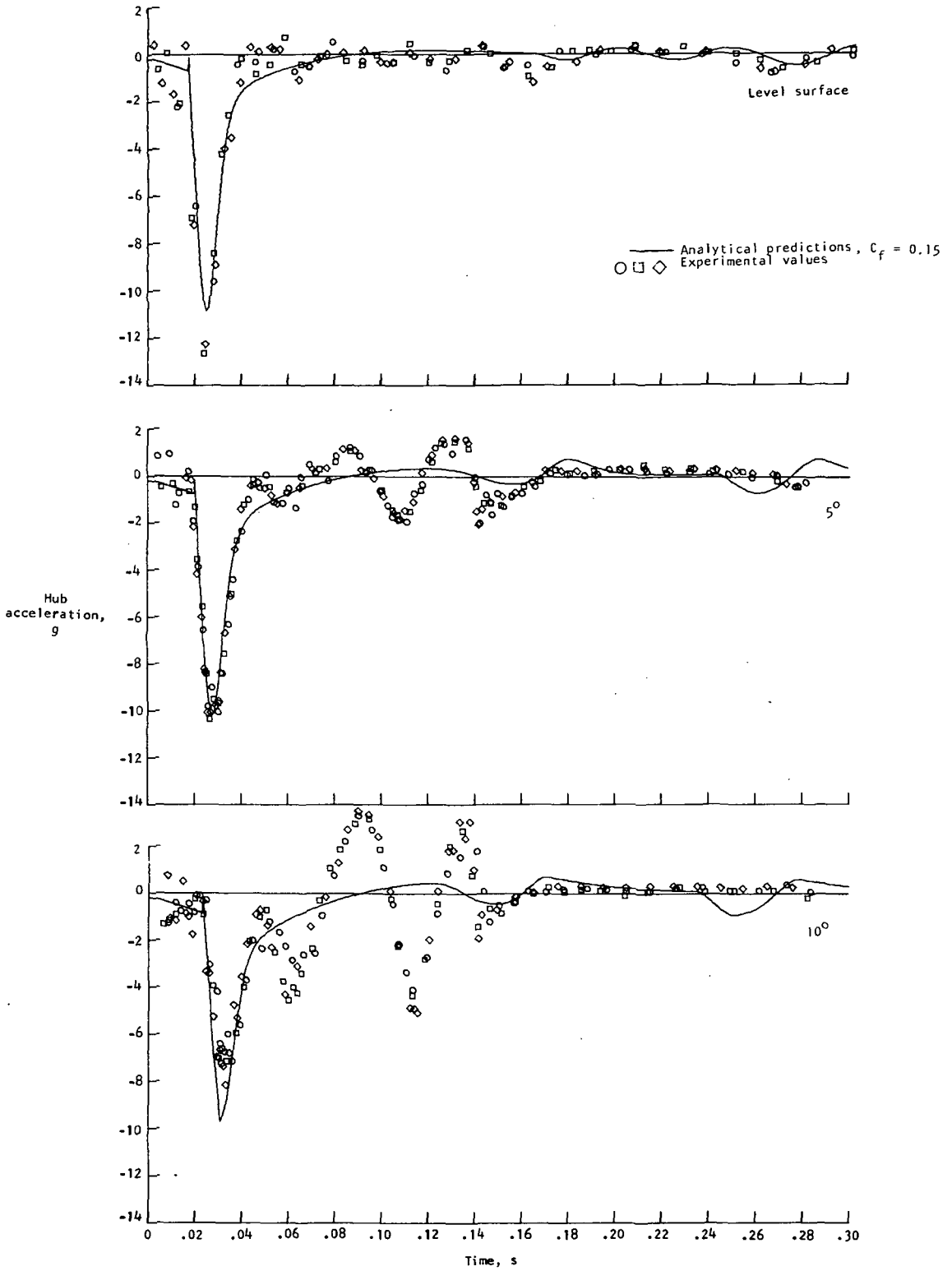

(e) Hub acceleration.

Figure 7.- Continued.

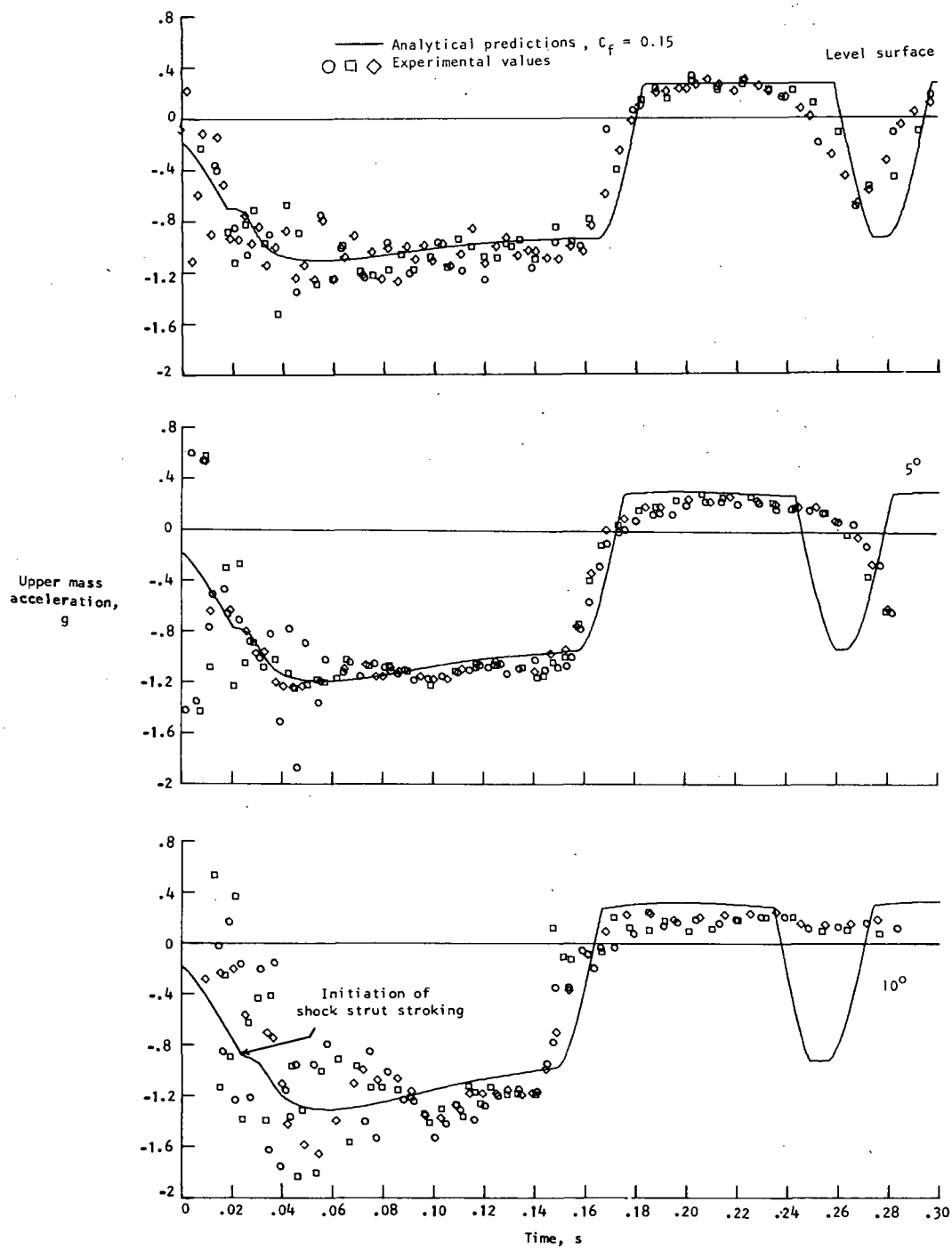

(f) Upper mass acceleration.

Figure 7.- Concluded.

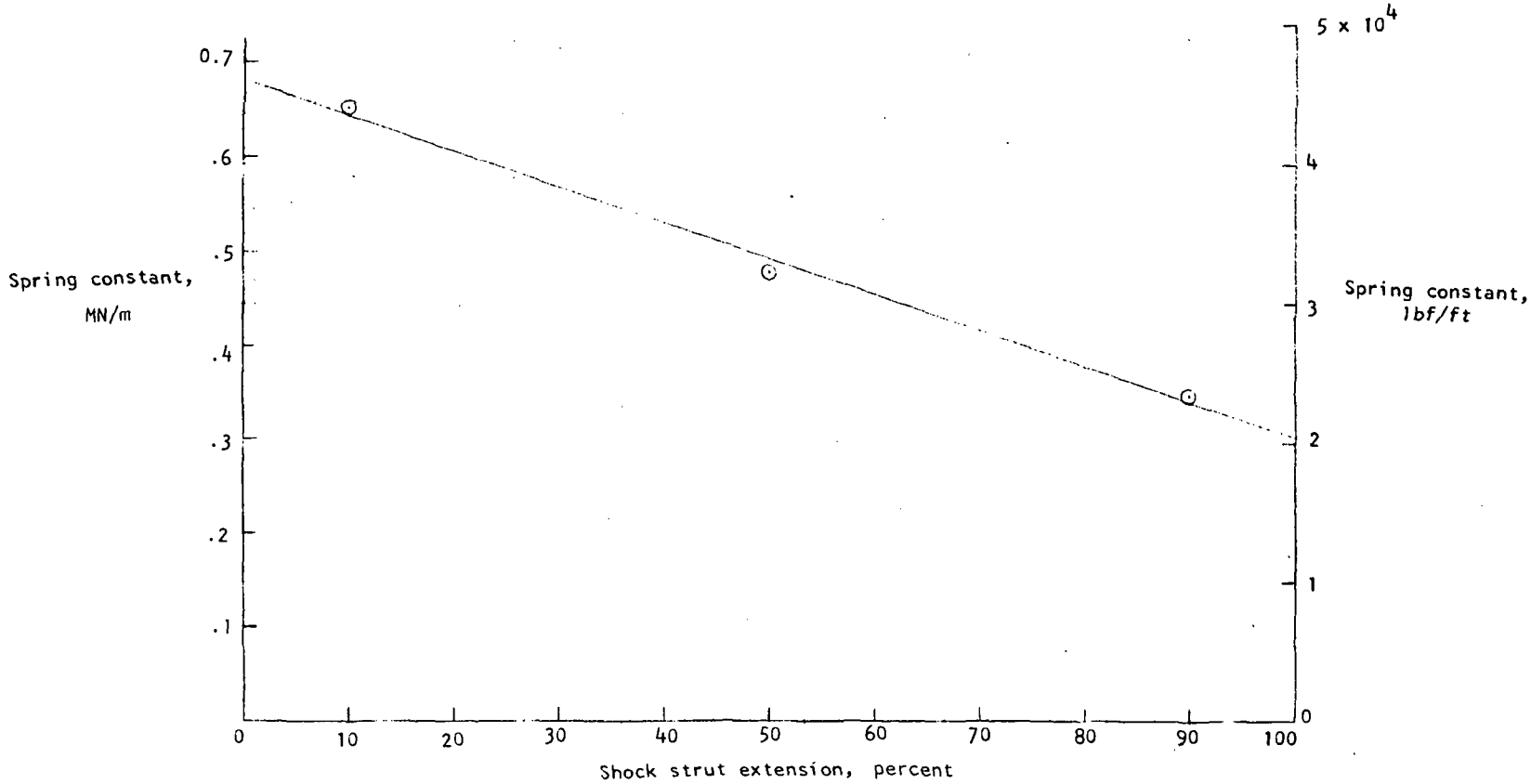

Figure 8.- Gear fore-and-aft spring constant as function of shock strut extension.

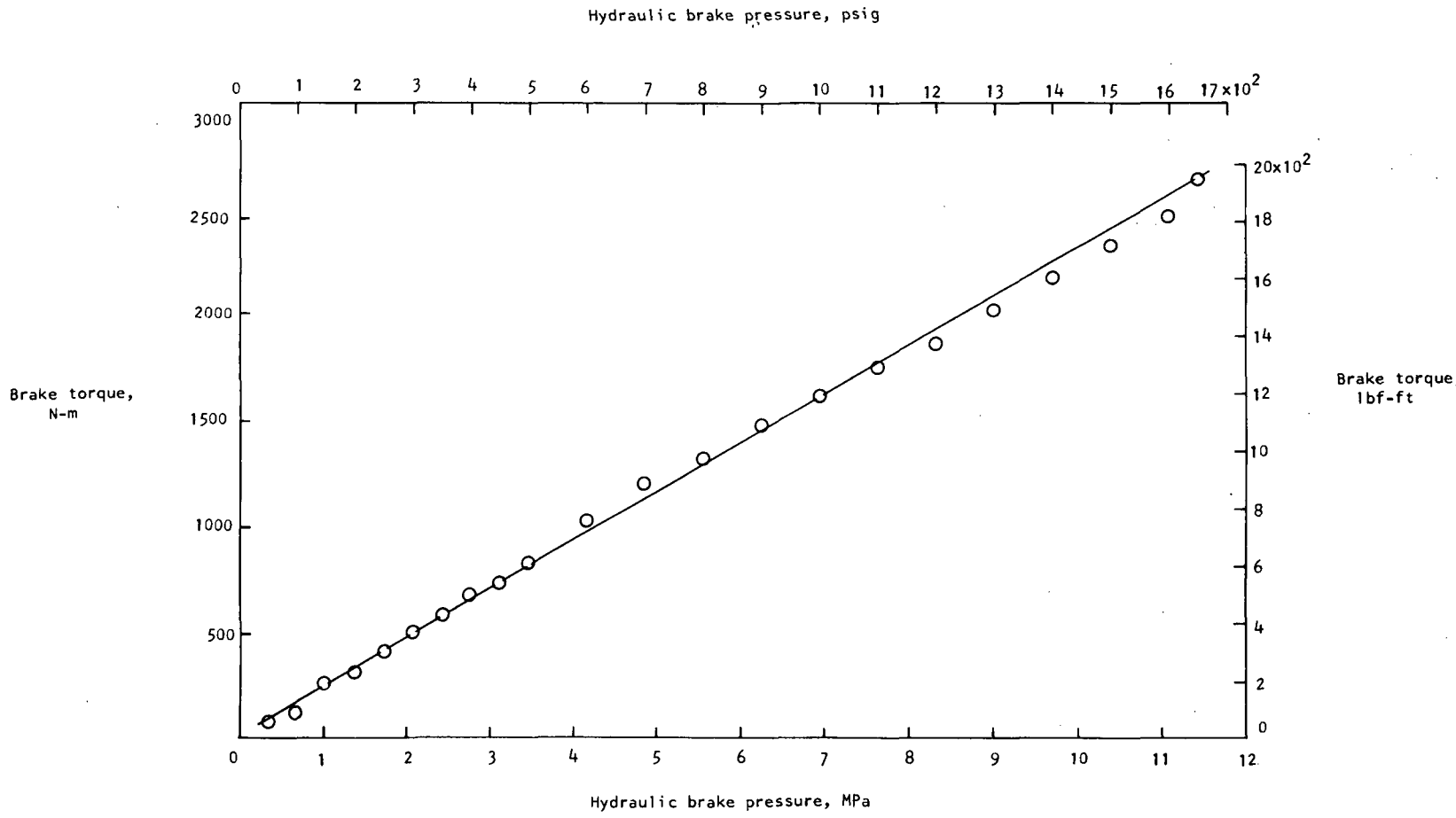

Figure 9.- Maximum brake torque as function of brake pressure.

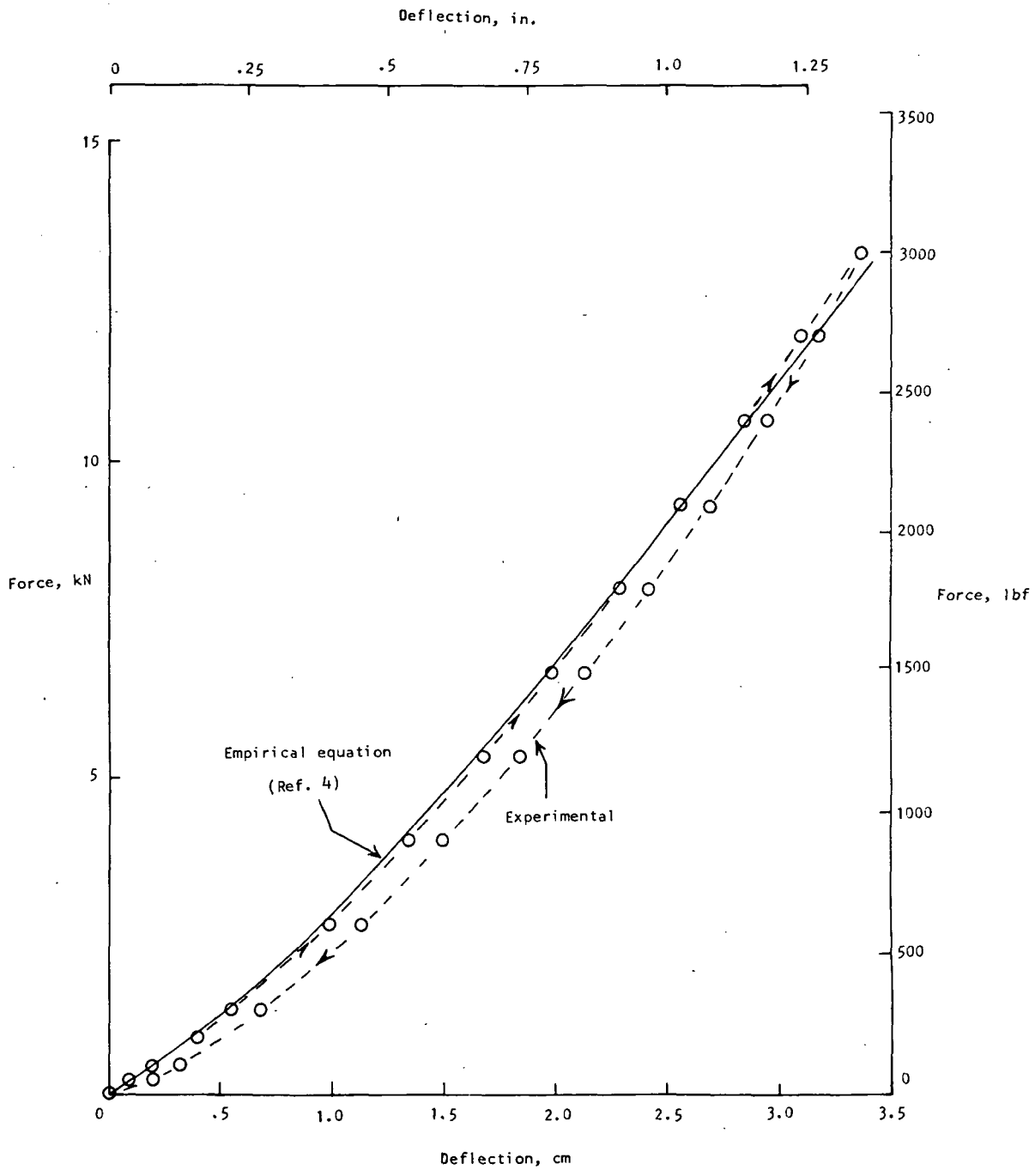

Figure 10.- Tire force as function of tire deflection.

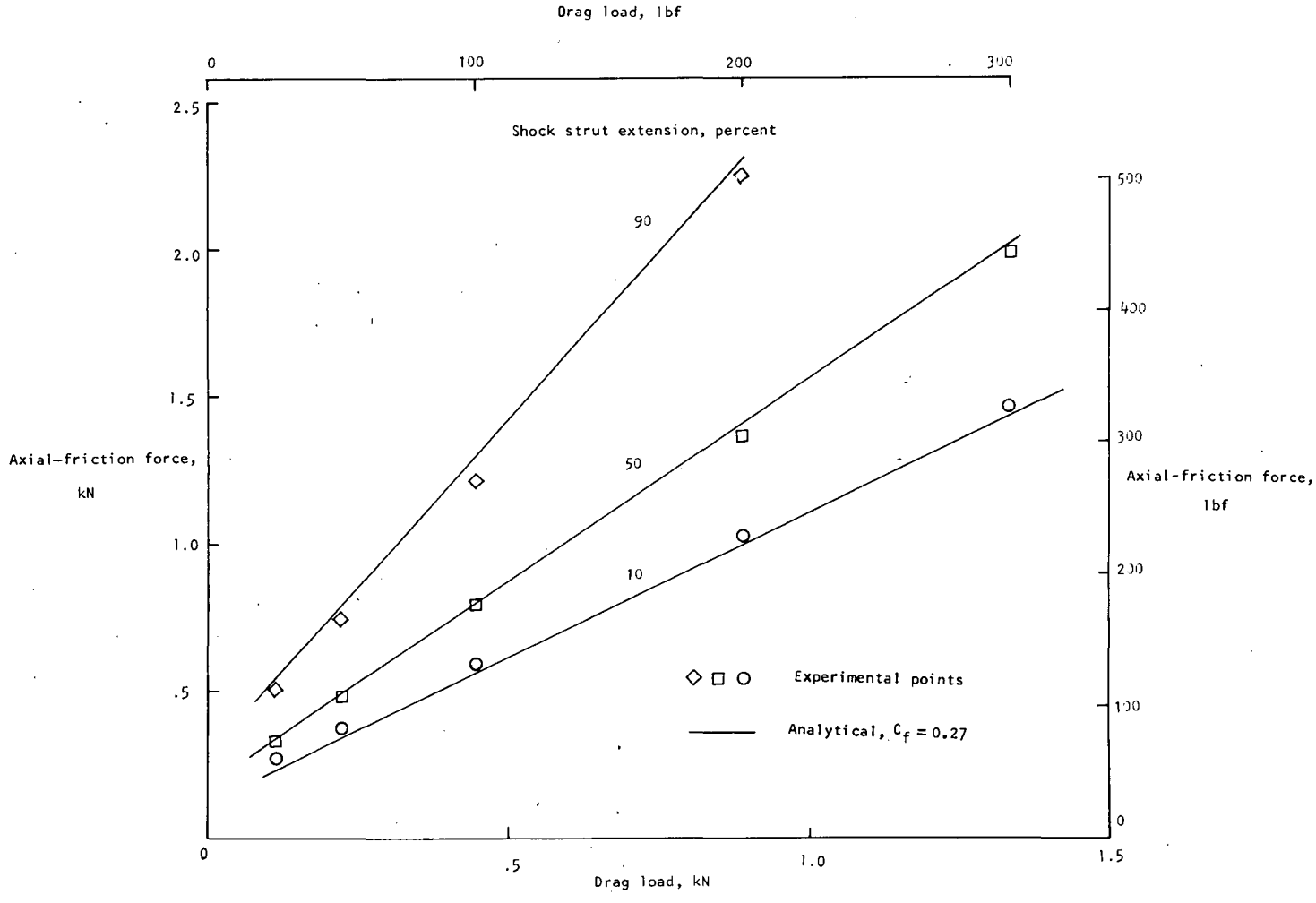

Figure 11.- Axial-friction force as function of drag load for 10-, 50-, and 90-percent extension of shock strut. C_f is bearing friction coefficient.

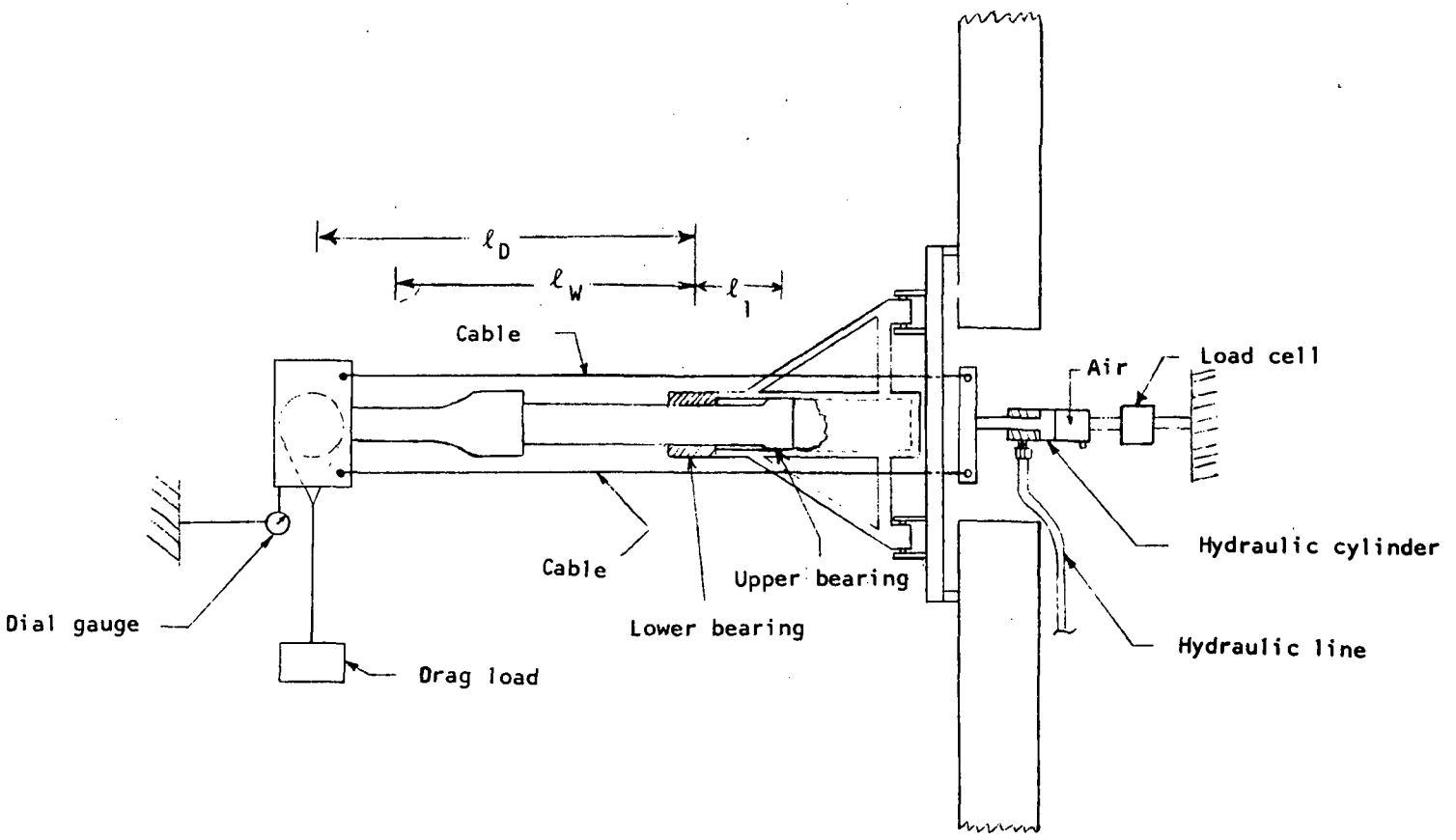

Figure 12.- Test setup for determining strut axial-friction coefficient and gear cantilever bending.

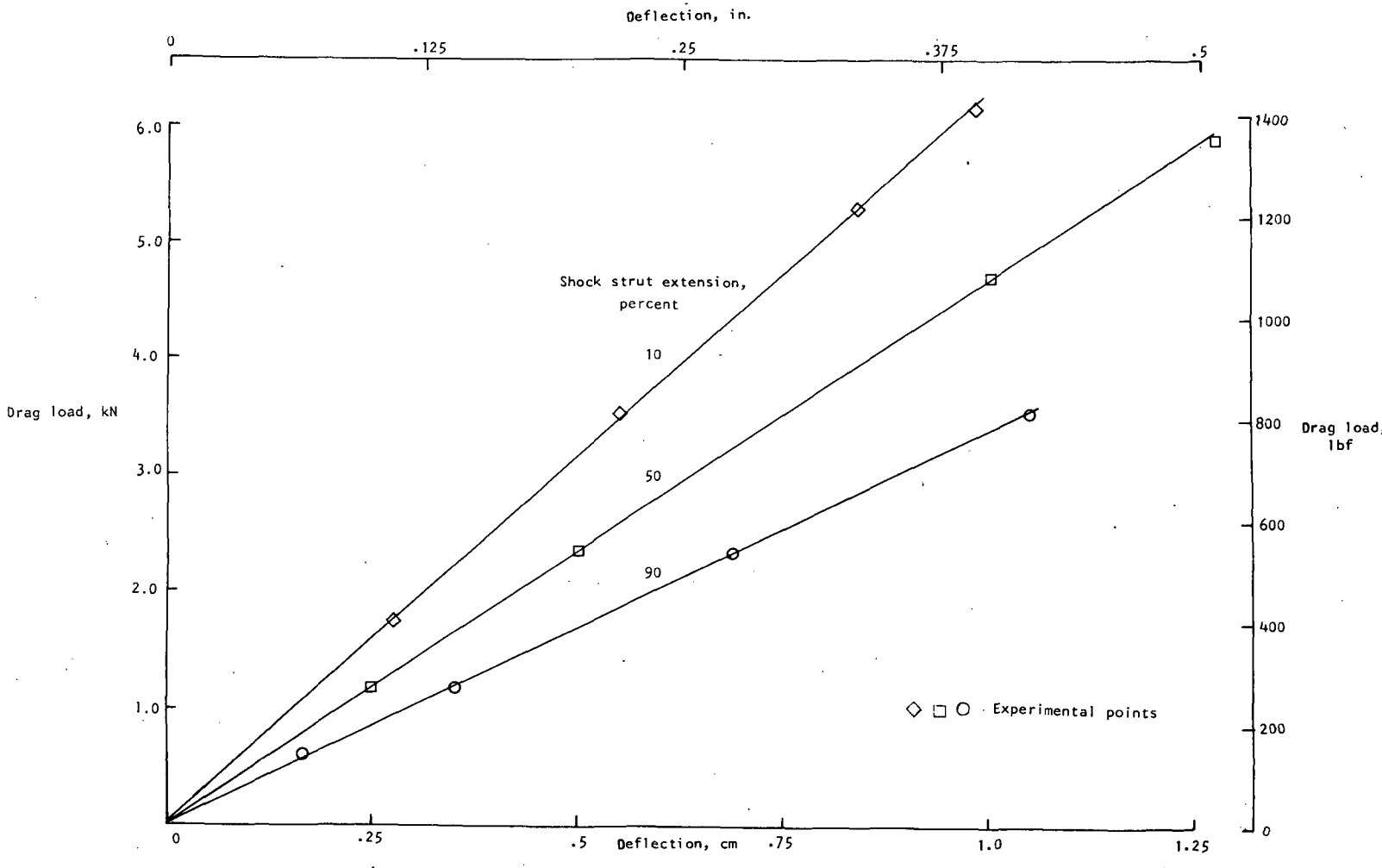

Figure 13.- Drag load as function of gear bending deflection.

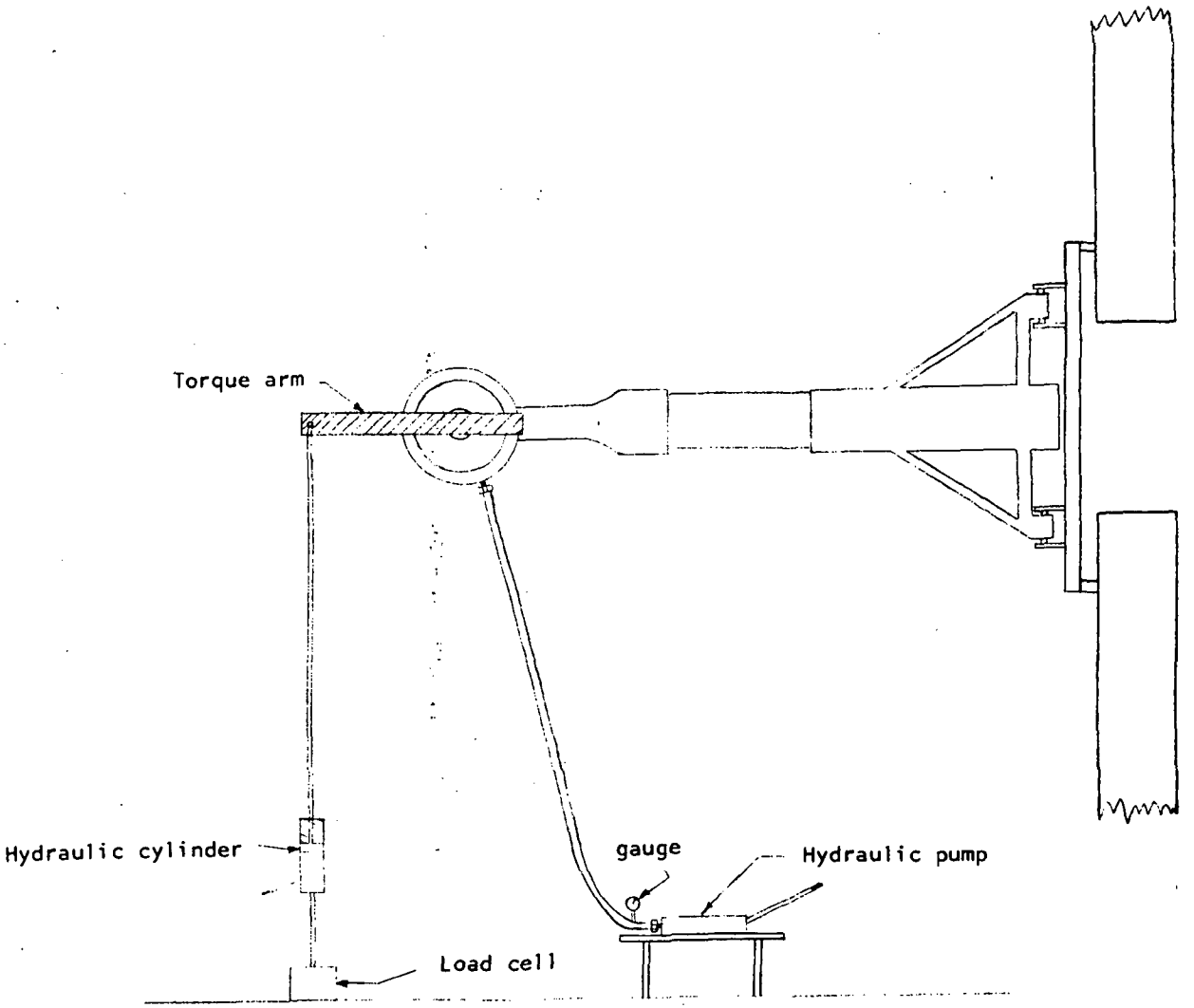

Figure 14.- Test setup for determining maximum brake torque as function of brake pressure.

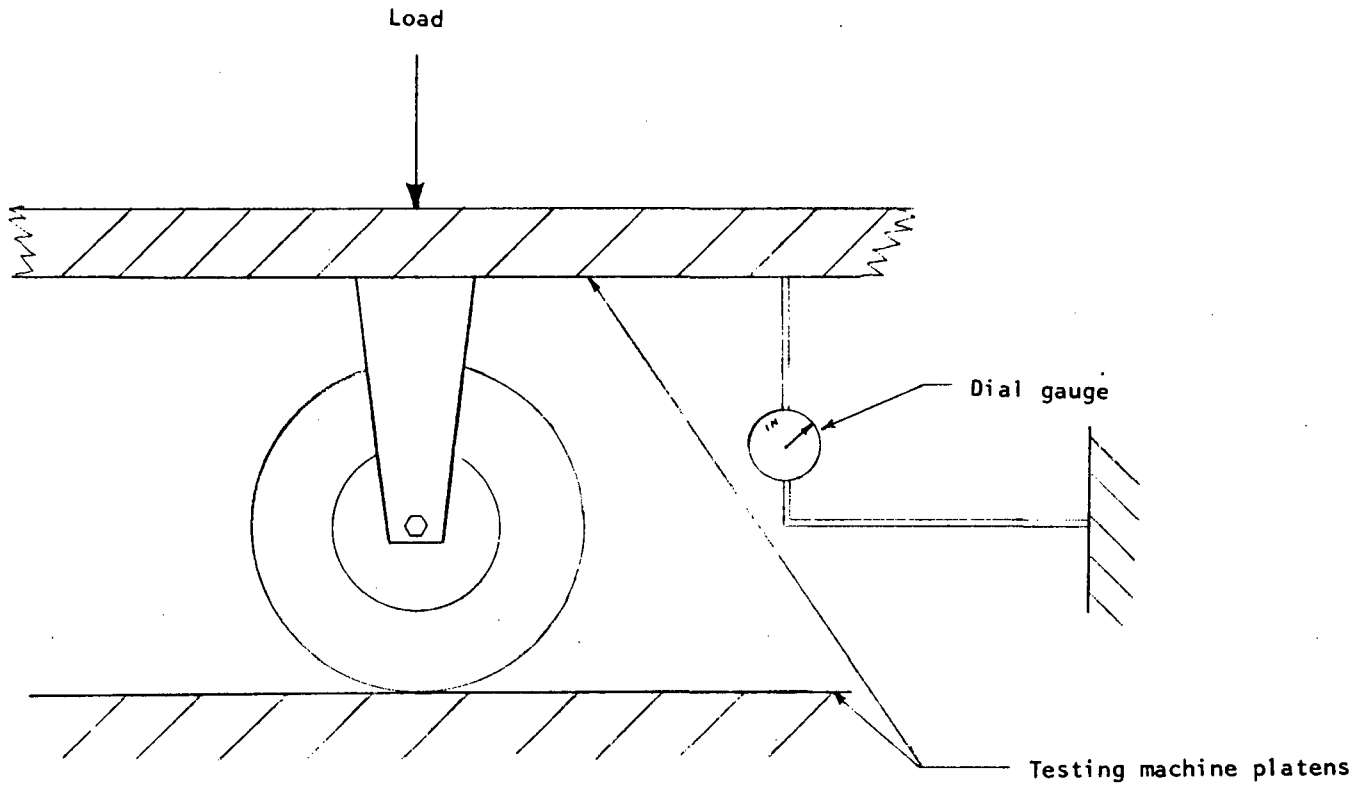

Figure 15.- Test setup for determining nonrotating tire force as function of deflection.

NATIONAL AERONAUTICS AND SPACE ADMINISTRATION
WASHINGTON, D.C. 20546

OFFICIAL BUSINESS
PENALTY FOR PRIVATE USE $300

THIRD-CLASS BULK RATE

POSTAGE AND FEES PAID
NATIONAL AERONAUTICS AND
SPACE ADMINISTRATION
451

U.S.MAIL

POSTMASTER: If Undeliverable (Section 158 Postal Manual) Do Not Return

"The aeronautical and space activities of the United States shall be conducted so as to contribute . . . to the expansion of human knowledge of phenomena in the atmosphere and space. The Administration shall provide for the widest practicable and appropriate dissemination of information concerning its activities and the results thereof."

—NATIONAL AERONAUTICS AND SPACE ACT OF 1958

NASA SCIENTIFIC AND TECHNICAL PUBLICATIONS

TECHNICAL REPORTS: Scientific and technical information considered important, complete, and a lasting contribution to existing knowledge.

TECHNICAL NOTES: Information less broad in scope but nevertheless of importance as a contribution to existing knowledge.

TECHNICAL MEMORANDUMS: Information receiving limited distribution because of preliminary data, security classification, or other reasons. Also includes conference proceedings with either limited or unlimited distribution.

CONTRACTOR REPORTS: Scientific and technical information generated under a NASA contract or grant and considered an important contribution to existing knowledge.

TECHNICAL TRANSLATIONS: Information published in a foreign language considered to merit NASA distribution in English.

SPECIAL PUBLICATIONS: Information derived from or of value to NASA activities. Publications include final reports of major projects, monographs, data compilations, handbooks, sourcebooks, and special bibliographies.

TECHNOLOGY UTILIZATION PUBLICATIONS: Information on technology used by NASA that may be of particular interest in commercial and other non-aerospace applications. Publications include Tech Briefs, Technology Utilization Reports and Technology Surveys.

Details on the availability of these publications may be obtained from:

SCIENTIFIC AND TECHNICAL INFORMATION OFFICE

NATIONAL AERONAUTICS AND SPACE ADMINISTRATION

Washington, D.C. 20546